RESEARCH ARTICLE SUMMARY

NEUROSCIENCE

Synaptotagmin-3 drives AMPA receptor endocytosis, depression of synapse strength, and forgetting

Ankit Awasthi*, Binu Ramachandran*, Saheeb Ahmed, Eva Benito, Yo Shinoda, Noam Nitzan, Alina Heukamp, Sabine Rannio, Henrik Martens, Jonas Barth, Katja Burk, Yu Tian Wang, Andre Fischer, Camin Dean†

INTRODUCTION: Memories are stored as molecular and cellular changes in the brain. Synapses, the nodes of connection between neurons, can store memories by virtue of their ability to tune the efficacy of communication between neurons. This property of synaptic plasticity makes it possible for the brain to store and retrieve memories—to replay patterns of electrical activity that occurred during an important event. Forgetting leads to the inability to retrieve memories by making them latent or decaying them below any useful quality. However, what determines whether a memory is forgotten? A mechanism is the regulation of neurotransmitter receptor numbers on the postsynaptic plasma membrane. These receptors mediate synaptic transmission by transducing presynaptically released neurotransmitters into an electrical signal. Neuronal activity strengthens synapses by inserting receptors or weakens synapses by removing receptors from the postsynaptic membrane. Receptor trafficking is controlled through calcium influx into the neuron; however, the calcium sensors mediating this control are not known.

RATIONALE: Synaptotagmin proteins sense calcium to trigger membrane fusion. Stimulating neuronal cultures elicits a calcium-mediated externalization of most synaptotagmin isoforms into plasma membranes, but synaptotagmin-3 (Syt3) internalizes from postsynaptic membranes. Stimulating AMPA (α-amino-3-hydroxy-5-methyl-4-isoxazolepropionic) or NMDA (*N*-methyl D-aspartate) receptors induces internalization of AMPA receptors (which mediate most of the fast synaptic transmission in the brain) and Syt3. This raised the intriguing possibility that Syt3 mediates activity-induced internalization of receptors to weaken synapses and cause forgetting. We imaged Syt3 using an isoform-specific antibody, tested its role in receptor trafficking using electrophysiological methods in brain slices and neuronal cultures, and tested its role in forgetting using spatial memory tasks in mice.

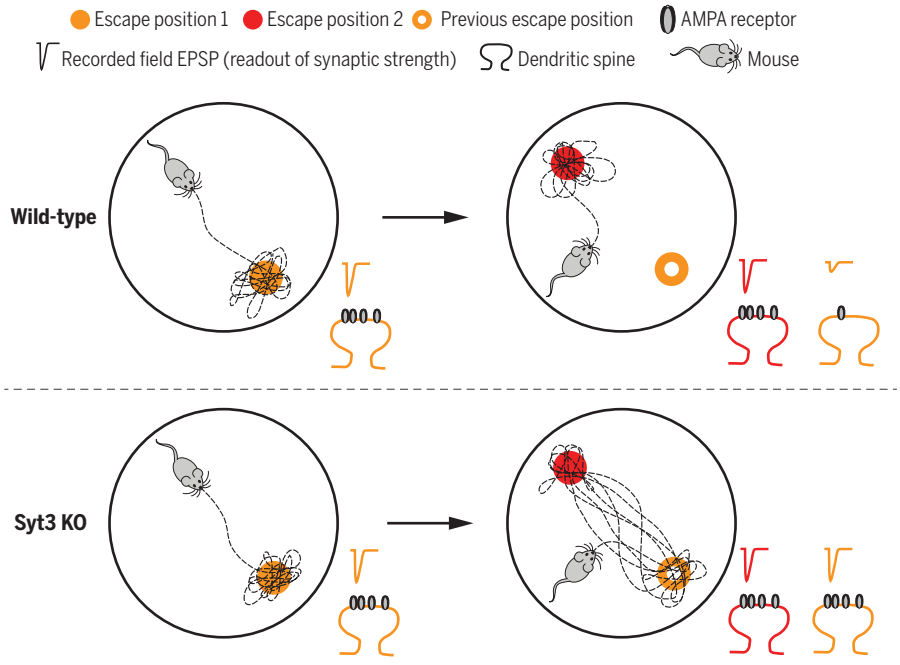

Syt3 knockout mice do not forget. Both wild-type mice and Syt3 knockout mice can learn an escape position in the water maze, in which corresponding synapses are strengthened through the increase of AMPA receptors. These synapses are weakened by the removal of receptors if the memory is no longer needed—for example, when a new escape position is learned. Syt3 knockout mice cannot remove receptors and therefore cannot forget previous escape positions.

RESULTS: Syt3 is on postsynaptic membranes at endocytic zones, which are clathrin-rich regions close to the postsynaptic density. Syt3 binds the GluA2 AMPA receptor subunit and also binds AP2 and BRAG2, two proteins implicated in activity-dependent internalization of AMPA receptors via clathrin-mediated endocytosis. Syt3 does not affect basal AMPA receptor trafficking. However, knocking out Syt3—or expressing calcium-binding–deficient Syt3—abolishes AMPA receptor internalization induced by AMPA, NMDA, or electrophysiological stimulation of long-term depression of synaptic strength. It also blocks the AMPA receptor internalization that normally decays long-term potentiation of synaptic strength. These effects are mimicked in a wild-type background through acute application of the Tat-GluA2-3Y peptide, which competitively inhibits binding of Syt3 to a tyrosine-rich (3Y) motif on the cytoplasmic tail of GluA2. In spatial memory tasks, mice in which Syt3 was knocked out (Syt3 knockout mice) learn escape positions normally but persevere to previously learned positions, which can be explained by a lack of forgetting previously acquired memories. Injecting the Tat-GluA2-3Y peptide in wild-type mice mimics the lack of forgetting of spatial memories, and this effect is occluded in Syt3 knockout mice.

ON OUR WEBSITE

Read the full article at http://dx.doi.org/10.1126/science.aav1483

CONCLUSION: The persistence or degradation of memories is governed by a poorly understood molecular machinery. We have discovered a distinct synaptotagmin isoform that triggers calcium-mediated internalization of AMPA receptors, resulting in a weakening of synaptic transmission and forgetting of spatial memories in mice. ■

The list of author affiliations is available in the full article online.
*These authors contributed equally to this work.
†Corresponding author. Email: c.dean@eni-g.de
Cite this article as A. Awasthi *et al.*, *Science* **363**, eaav1483 (2019). DOI: 10.1126/science.aav1483

RESEARCH ARTICLE

NEUROSCIENCE

Synaptotagmin-3 drives AMPA receptor endocytosis, depression of synapse strength, and forgetting

Ankit Awasthi[1]*, Binu Ramachandran[1]*, Saheeb Ahmed[1]†, Eva Benito[2,3], Yo Shinoda[1]‡, Noam Nitzan[1], Alina Heukamp[1]§, Sabine Rannio[1], Henrik Martens[4], Jonas Barth[2,3], Katja Burk[1], Yu Tian Wang[5], Andre Fischer[2,3], Camin Dean[1]¶

Forgetting is important. Without it, the relative importance of acquired memories in a changing environment is lost. We discovered that synaptotagmin-3 (Syt3) localizes to postsynaptic endocytic zones and removes AMPA receptors from synaptic plasma membranes in response to stimulation. AMPA receptor internalization, long-term depression (LTD), and decay of long-term potentiation (LTP) of synaptic strength required calcium-sensing by Syt3 and were abolished through Syt3 knockout. In spatial memory tasks, mice in which Syt3 was knocked out learned normally but exhibited a lack of forgetting. Disrupting Syt3:GluA2 binding in a wild-type background mimicked the lack of LTP decay and lack of forgetting, and these effects were occluded in the Syt3 knockout background. Our findings provide evidence for a molecular mechanism in which Syt3 internalizes AMPA receptors to depress synaptic strength and promote forgetting.

A fundamental property of the brain is the ability to learn from experience by modulating the strength of synaptic connections between neurons. The trafficking of AMPA receptors to and from the surface of postsynaptic membranes is a key determinant in the regulation of synaptic strength (*1*–*3*). High-frequency stimulation increases surface receptors and promotes long-term potentiation (LTP) of synaptic strength. Low-frequency stimulation removes receptors from the postsynaptic membrane and causes long-term depression (LTD) of synaptic strength. This phenomenon has been most extensively studied in *N*-methyl-D-aspartate (NMDA)–receptor–dependent plasticity of CA3-CA1 synapses in the hippocampus (*4*). LTP is widely believed to underlie learning (*5*–*7*). Conversely, weakening of potentiated synapses, and LTD, can promote forgetting (*5*, *8*, *9*).

Both LTD (*10*, *11*) and the decay of LTP depend on activity-dependent removal of postsynaptic GluA2-containing AMPA receptors from the plasma membrane (*8*, *12*, *13*). Ca^{2+} influx into dendrites is critical for virtually all types of synaptic plasticity (*4*), including decay of LTP (*14*, *15*) and active internalization of GluA2-containing AMPA receptors (*16*, *17*). The same signaling entity can have divergent consequences for the synapse: Fast, high [Ca^{2+}] influx can promote LTP, whereas gradual, low [Ca^{2+}] influx can promote LTD (*4*). Plasma membrane–localized Ca^{2+}-binding proteins are likely needed to remove or add receptors to the postsynaptic membrane through regulated endo- or exocytosis. Synaptotagmins (Syts) are candidates for such a function (*18*). This family of integral membrane proteins contain a short luminal tail, transmembrane domain, and two conserved cytoplasmic Ca^{2+}-binding C2 domains (*19*) that regulate Ca^{2+}-dependent membrane recycling events.

Of the 17 mammalian Syt isoforms, Syt3 is the third most abundant in the brain. Unlike Syt1 and Syt2, which are predominantly thought to be localized to synaptic vesicle membranes, Syt3 was reported to be localized to the plasma membrane (*20*, *21*) and to have a 10-fold higher Ca^{2+} affinity than that of Syt1 and Syt2 (*22*). In a pHluorin-Syt screen of Syt isoforms in response to stimulation, Syt3 exhibited distinct recycling properties: It was the only isoform to endocytose in response to stimulation and to recycle exclusively in dendrites (*23*). Because the kinetics of stimulus-induced pHluorin-Syt3 endocytosis resembled those of pHluorin-GluA2 (*24*, *25*), we hypothesized that Syt3 may regulate Ca^{2+}- and activity-dependent postsynaptic receptor endocytosis to affect synaptic plasticity.

[1]Trans-synaptic Signaling Group, European Neuroscience Institute, 37077 Goettingen, Germany. [2]German Center for Neurodegenerative Disease, 37075 Goettingen, Germany. [3]Department of Psychiatry and Psychotherapy, University Medical Center Goettingen, 37075 Goettingen, Germany. [4]Synaptic Systems GmbH, 37079 Goettingen, Germany. [5]Brain Research Center and Department of Medicine, University of British Columbia, Vancouver, BC V6T2B5, Canada.
*These authors contributed equally to this work.
†Present address: Department of Diagnostic and Interventional Radiology, University Medical Center Goettingen, 37075 Goettingen, Germany.
‡Present address: Department of Environmental Health, School of Pharmacy, Tokyo University of Pharmacy and Life Sciences, Tokyo 192-0392 Japan. §Present address: Department of Neurobiology, Weizmann Institute of Science, 7610001 Rehovot, Israel.
¶**Corresponding author. Email: c.dean@eni-g.de**

Results

Syt3 is on postsynaptic plasma membranes

To examine the location of Syt3, we developed a highly specific antibody (fig. S1, A and B) that recognized a single band in brain homogenates, which was absent in Syt3 knockouts; an antibody developed by Neuromab showed similar results (Fig. 1A). Syt3 was most abundant in adipose tissue, heart, and brain (fig. S1C), where it was found in the hippocampus, cortex, thalamus, and striatum (fig. S1D). Expression in the brain began embryonically and remained high throughout adulthood (fig. S1E). Immunostains revealed Syt3 signal on neuronal cell bodies and dendrites in the CA1 (Fig. 1B), CA3, and dentate gyrus (fig. S1F) in wild-type, but not Syt3 knockout, hippocampal slices.

To localize Syt3 subcellularly, we expressed cytosolic green fluorescent protein (GFP) in cultured hippocampal neurons and immunostained for Syt3 and MAP2 to distinguish dendrites (MAP2-positive) from axons (GFP-positive/MAP2-negative). Syt3 signal was predominantly detected in dendrites (90.2 ± 3.0% of total signal) compared with axons (9.8 ± 5.1% of total signal) ($P < 0.001$) (Fig. 1C). Syt3 exhibited a punctate pattern in dendrites and colocalized with the pre- and postsynaptic markers synaptophysin, and PSD95 or GluA1, respectively, at synapses (Fig. 1D); 70.6 ± 5.3% of Syt3 signal was at excitatory synapses (fig. S1G), and 29.4 ± 1.9% was at inhibitory synapses ($P < 0.001$) (fig. S1H). In subcellular fractions, Syt3 was associated with synaptosomal plasma membranes and not with synaptic vesicles (fig. S1I), which is in agreement with a previous report (*20*). Immuno-organelle isolation of synaptic vesicles with antibodies to Syt1 or Syb2 further confirmed that Syt3 is not present on synaptic vesicles (fig. S1J). We further tested whether Syt3 is specifically localized to postsynaptic membranes using a trypsin cleavage assay of synaptosomes (*26*). Synaptosomes form in such a way that the presynaptic terminal seals, trapping synaptic vesicles and other presynaptic components inside (Fig. 1E), whereas the postsynaptic membrane does not reseal. Presynaptic proteins were therefore protected from trypsin cleavage, whereas postsynaptic proteins, including Syt3, were cleaved (Fig. 1F).

Stimulation induces endocytosis of Syt3

The presence of Syt3 on postsynaptic membranes suggests it may regulate a post-synaptic recycling event. Time-lapse imaging of pHluorin-Syt3 in transfected hippocampal neurons during depolarization with 45 mM KCl (*23*) or field stimulation revealed a calcium-dependent fluorescence decrease, requiring NMDA/AMPA receptors and L-type calcium channels, likely corresponding to endocytosis (fig. S2, A to D). PHluorin-Syt3 also exhibited calcium-dependent endocytosis in response to AMPA (Fig. 2A) and NMDA (Fig. 2B)—stimuli that promote AMPA receptor internalization—with kinetics similar to those of pHluorin-tagged AMPA receptors (*24*, *25*).

Because interpretation of pHluorin experiments may be confounded by intracellular acidification

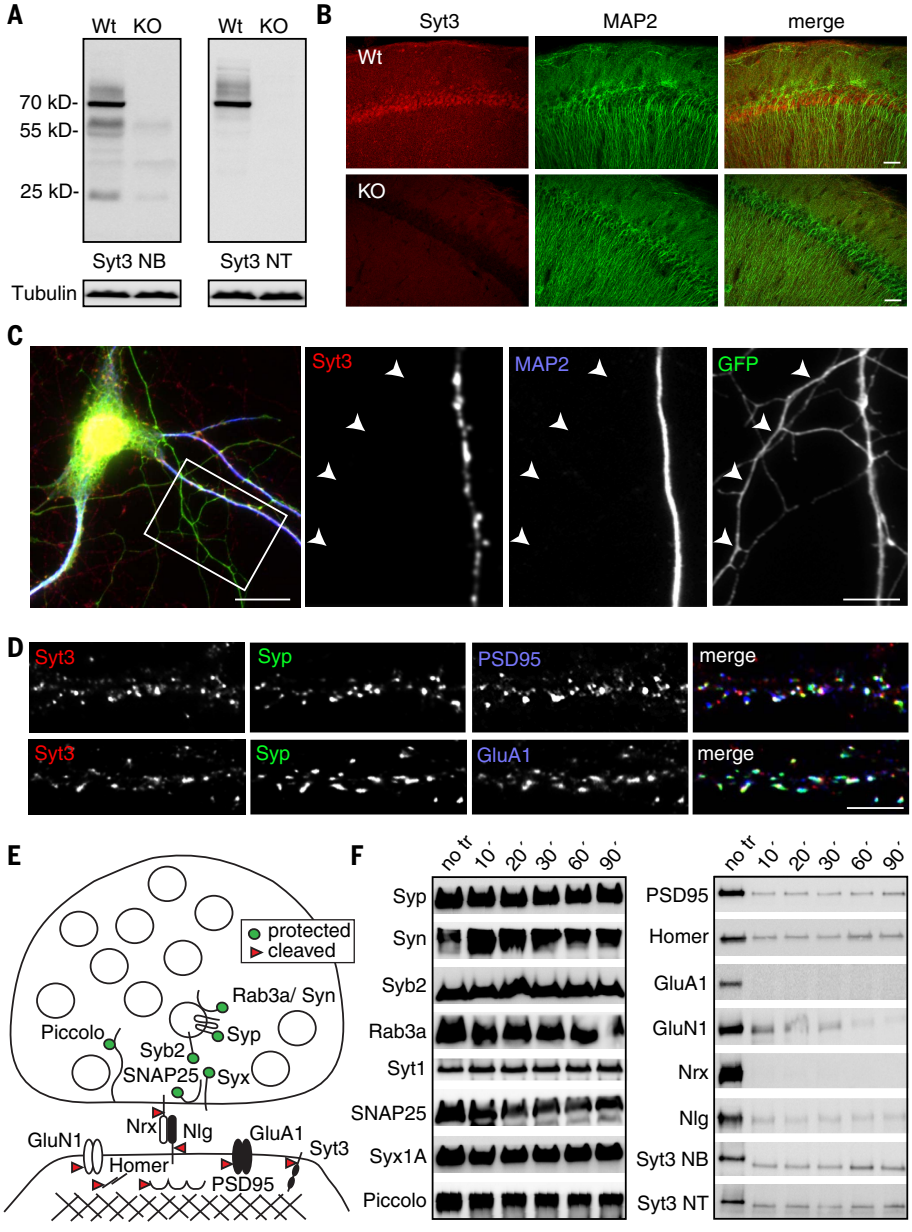

Fig. 1. Syt3 is postsynaptic. (**A**) Syt3 antibodies recognize a specific band of the expected molecular weight in wild-type (WT) but not in Syt3 knockout (KO) mouse brain homogenates in Western blots. Syt3 NB is a monoclonal antibody from Neuromab, and Syt3 NT is a polyclonal antibody developed by Synaptic Systems. Tubulin is a loading control. (**B**) Syt3 immunoreactivity is detected on pyramidal cell bodies and dendrites in the CA1 region of hippocampal slices but not in Syt3 knockouts. MAP2 marks dendrites. Scale bar, 50 μm. (**C**) Syt3 is predominantly in dendrites in hippocampal neurons transfected with GFP and immunostained with MAP2 to mark dendrites (MAP2-positive) or axons (GFP-positive/MAP2-negative) (n = 20 neurons/3 cultures). Scale bar, 20 μm (left), 5 μm (right). (**D**) Syt3 localizes to synapses marked by synaptophysin and PSD95 (top) or GluA1 (bottom) in hippocampal cultures. Scale bar, 5 μm. (**E**) Schematic of a synaptosome. The presynaptic side reseals, whereas the postsynaptic side does not, leaving postsynaptic proteins accessible to trypsin cleavage. (**F**) Presynaptic proteins are protected from trypsin cleavage, whereas postsynaptic proteins (including Syt3) are cleaved.

in response to AMPA and NMDA stimulation (*27*), we performed an additional assay to test internalization of Syt3. We expressed GFP-Syt3 in Syt3 knockout neurons and labeled surface GFP-Syt3 with an antibody to GFP, stimulated neurons with AMPA or NMDA, and then labeled remaining surface GFP-Syt3 with a secondary antibody of one color, permeabilized cells, and labeled internalized GFP-Syt3 with a secondary antibody of another color so as to quantify Syt3 internalized in response to stimulation. We found a significant increase in internalized GFP-Syt3 after stimulation with AMPA and NMDA compared with that in control conditions (Fig. 2C).

AMPA receptor endocytosis is thought to occur at postsynaptic endocytic zones—marked by fluorescently tagged Clathrin light chain—which is adjacent to, but distinct from, postsynaptic densities marked by fluorescently tagged Homer (*28*–*31*). To visualize these markers exclusively at postsynaptic sites, neuronal cultures were sparsely transfected so that dendrites of transfected neurons can be identified and fluorescent marker colocalization quantified at postsynaptic sites in these dendrites. We first verified that Clathrin and Homer can be distinguished; only 4.4 ± 1.1% of Clathrin light chain-DsRed and Homer-myc puncta overlapped (Fig. 2D). We further found that only 4.0 ± 1.3% of GFP-Syt3 puncta colocalized with Homer-myc at postsynaptic densities, whereas 84.0 ± 1.8% of GFP-Syt3 puncta in dendrites colocalized with Clathrin-DsRed at endocytic zones (Fig. 2D).

Syt3 internalizes AMPA receptors

Does Syt3 endocytose receptors? As a first test, we pulled down binding partners of Syt3 from brain homogenates. Recombinant Syt3 pulled down GluA2 but not other receptor subunits and also pulled down the endocytic proteins AP-2 (*32*) and BRAG2 (*10*)—two proteins implicated in receptor endocytosis—but not GRIP or PICK1 (Fig. 2E and fig. S3), which bind distinct regions of the GluA2 C-terminal tail (Fig. 2F) (*1*). Syt3 bound GluA2 in a calcium-dependent manner and bound AP-2 and BRAG2 in the absence of calcium, and at concentrations up to 10 μM in the case of AP2 (Fig. 2G). Because the nine–amino acid 3Y tail of GluA2 is important for receptor internalization, we tested whether Syt3 interacts with this region. Incubation of brain lysates with 1 μM Tat-GluA2-3Y peptide—which competitively inhibits protein binding to the GluA2 3Y region and blocks activity-dependent endocytosis of receptors (*10*, *13*)—indeed disrupted Syt3:GluA2 binding (Fig. 2H).

Because Syt3 pulled down GluA2 receptors, and GluA1/GluA2 heteromers comprise the majority of AMPA receptors in the hippocampus (*33*), we examined internalization of GluA1- and GluA2-containing receptors in response to stimulation (*17*, *32*, *34*) in dissociated hippocampal neurons in which Syt3 was overexpressed or knocked down postsynaptically, using sparse transfection. Surface epitopes of GluA1 or GluA2 in hippocampal cultures were labeled with primary antibodies, followed by stimulation with AMPA or NMDA to promote receptor internalization. Surface receptors were then labeled with a secondary antibody of one color and internalized receptors labeled with a second color after permeabilization, whereby the ratio of internal/surface signal reports the extent of receptor internalization. Overexpression of GFP-Syt3 increased internalization of GluA1 and GluA2, whereas Syt3 knockdown or expression of a calcium-binding–deficient mutant of Syt3 abolished stimulation-induced internalization of

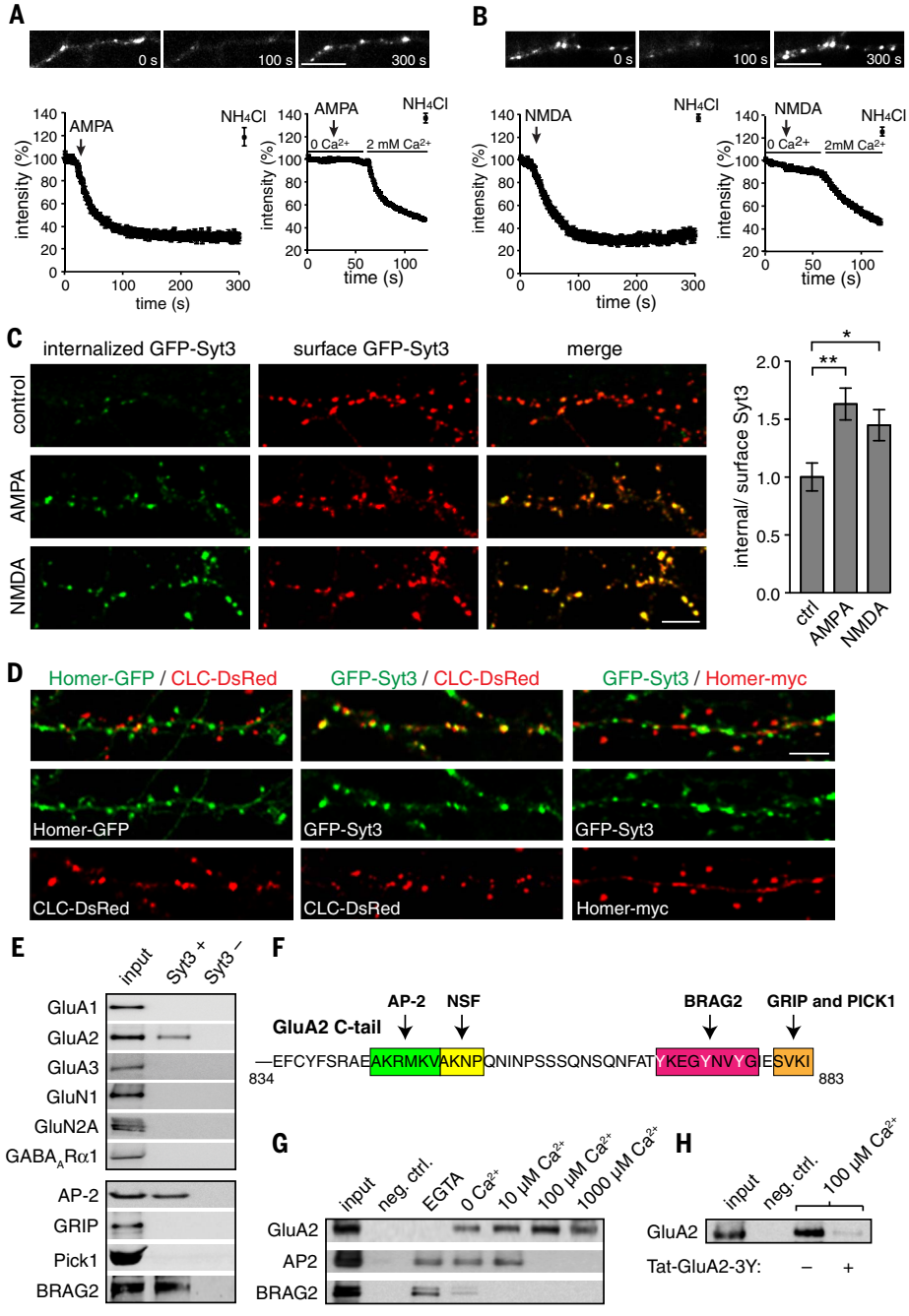

Fig. 2. Syt3 endocytoses in response to stimulation and binds GluA2, AP-2, and BRAG2. (**A**) pHluorin-Syt3 endocytoses in response to stimulation with AMPA or NMDA (**B**) in 2 mM calcium (left), but not in the absence of calcium (right) [*n*; ROI/neurons/cultures, AMPA 2 mM Ca^{2+} 37/7/3 (left); 0 and 2 mM Ca^{2+} 42/6/3 (right); NMDA, 2 mM Ca^{2+} 35/3/3 (left); 0 and 2 mM Ca^{2+} 40/3/3 (right)]. NH_4Cl dequenches internalized pHluorin-Syt3 fluorescence. Scale bars, 5 μm. (**C**) GFP-Syt3 expressed in Syt3 knockout hippocampal neurons internalizes in response to stimulation with AMPA and NMDA (*n* = 28, 25, and 26 neurons per 2 cultures for control, AMPA, and NMDA, respectively; one-way ANOVA, Tukey's test). (**D**) GFP-Syt3 colocalizes with CLC (clathrin light chain)–Dsred at postsynaptic endocytic zones, and not with Homer-myc at PSDs (*n*; ROI/neurons, 34/20 Homer-GFP/CLC-DsRed; 29/19 GFP-Syt3/CLC-Dsred; 34/18 GFP-Syt3/Homer-myc from three cultures). Scale bars, 5 μm. (**E**) Recombinant Syt3 C2AB pulls down GluA2, AP2, and BRAG2 from brain homogenates. Syt3– is beads only. (**F**). Binding sites, on the GluA2 C-terminal tail, of proteins implicated in receptor recycling and tested in pull downs. (**G**) Calcium-dependence of Syt3 C2AB pull down of GluA2, AP2, and BRAG2 from brain homogenate. In 0 Ca^{2+} conditions, brains were homogenized and solubilized in calcium-free buffer, but endogenous buffered calcium in internal stores remains. Addition of EGTA eliminates any potential effects of these additional sources of calcium. (**H**) Western blot of GluA2 pulled down from brain homogenate by Syt3 C2AB in 100 μM calcium with or without preincubation with 1 μM Tat-GluA2-3Y peptide. Negative controls are beads only.

receptors [Fig. 3, A to C, and fig. S4, A to D; Syt3 short hairpin RNA (shRNA) knockdown validation is provided in fig. S4, E and F]. Manipulation of Syt3 did not affect surface versus internal receptors in basal conditions. Syt3 knockout neurons yielded similar results; GluA2 receptors were internalized in response to AMPA and NMDA stimulation in wild-type neurons but not in Syt3 knockout neurons or in wild-type neurons treated with the Tat-GluA2-3Y peptide (Fig. 3, D and E, and fig. S4G).

Syt3 does not affect basal transmission

We found no change in miniature excitatory postsynaptic current (mEPSC) amplitude, frequency, or decay time in Syt3 overexpressing or knockdown neurons compared with GFP-transfected controls (decay time GFP, 2.3 ± 0.2 ms; GFP-Syt3, 2.1 ± 0.2 ms; Syt3 KD, 1.9 ± 0.2 ms) (fig. S5, A to D), further confirming that postsynaptic Syt3 does not affect surface receptor number in basal conditions. To exclude presynaptic effects, we also compared mEPSCs in wild-type and Syt3 knockout cultures and again found no difference in mEPSC amplitude or frequency (frequency $P = 0.2671$; t test, Welch's correction) (fig. S5, E to G). After stimulation, however, mEPSC amplitude decreased in wild-type but not in Syt3 knockout neurons, and this effect was rescued by reintroducing GFP-Syt3 postsynaptically into knockout neurons (fig. S5H), confirming a lack of stimulation-induced internalization of synaptic AMPA receptors in Syt3 knockouts.

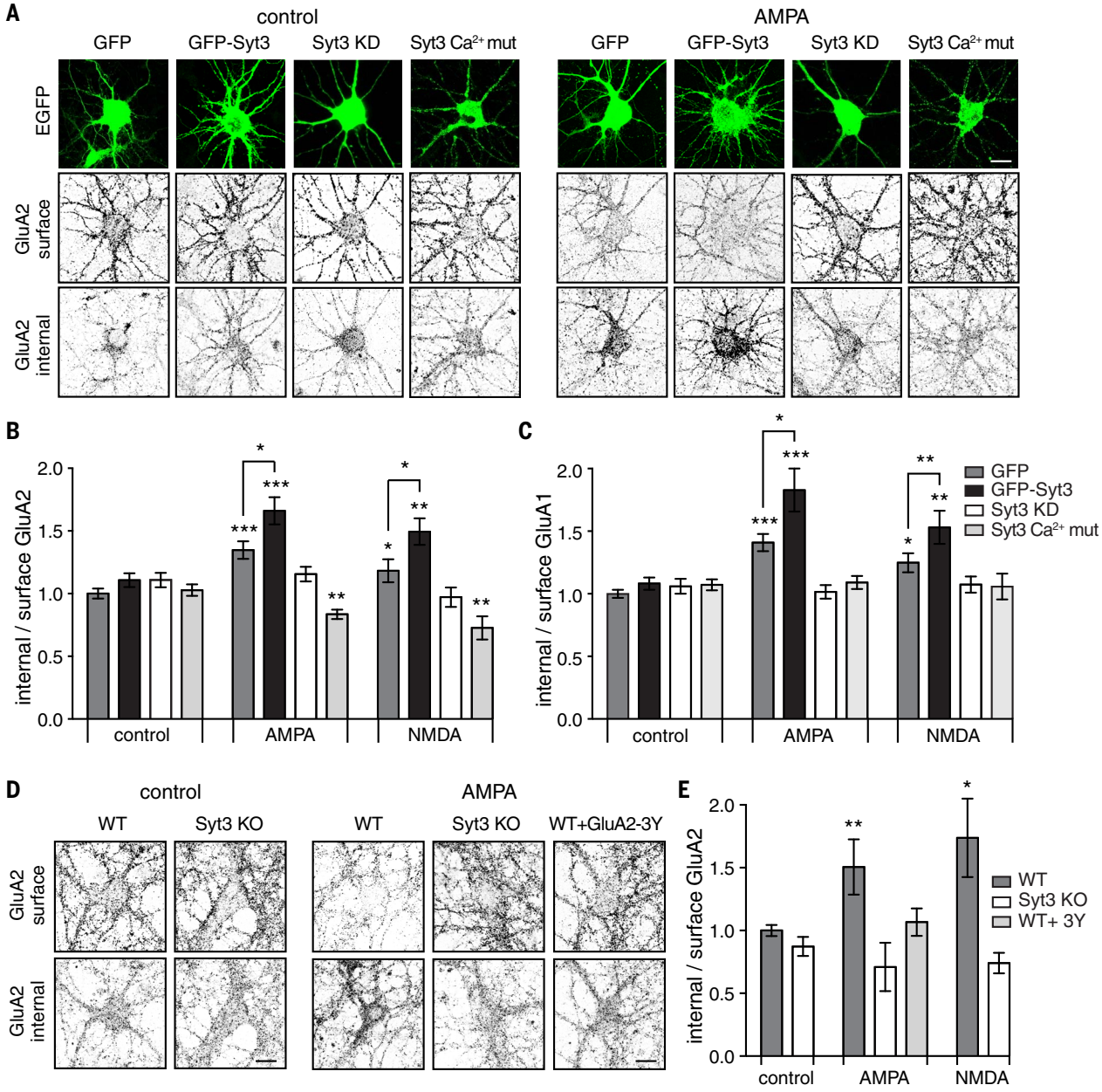

Fig. 3. Syt3 internalizes AMPA receptors in response to stimulation. (**A**) Hippocampal neurons transfected with GFP, GFP-Syt3, Syt3 knockdown (Syt3 KD), or Syt3 calcium-binding deficient mutant (Syt3 Ca^{2+} mut) constructs in control and AMPA-stimulated conditions, immunostained for surface and internalized GluA2 receptors. (**B**) Stimulation-induced GluA2 and GluA1 (**C**) internalization is increased by overexpression of GFP-Syt3 and blocked by Syt3 KD or Syt3 Ca^{2+} mut (*n*; neurons for GluA2/GluA1; GFP, 64/69 ctrl, 68/46 AMPA, 28/47 NMDA; GFP-Syt3, 46/65 ctrl, 46/47 AMPA, 23/43 NMDA; Syt3 KD, 51/41 ctrl, 69/38 AMPA, 23/24 NMDA; Syt3 Ca^{2+} mut, 42/37 ctrl, 28/36 AMPA, 27/31 NMDA from six cultures). (**D** and **E**) Stimulation-induced GluA2 internalization is abolished in Syt3 knockout neurons, and in WT neurons treated with the Tat-GluA2-3Y peptide (*n*; Syt3 KO/WT neurons, 31/29 ctrl, 24/22 AMPA, 18/17 NMDA; WT+GluA2-3Y, 18 AMPA, from four cultures). Scale bars, 10 μm; two-way ANOVA, Dunnett's test.

Basal synaptic transmission was also unchanged in Syt3 knockouts. Recordings of synaptic responses from CA1 neurons, elicited by Schaffer collateral stimulation in acute hippocampal slices, displayed no change in NMDA/AMPA, γ-aminobutyric acid (GABA)/AMPA, or GABA/NMDA receptor–mediated response ratio in Syt3 knockout compared with wild-type neurons (fig. S5, I to L). There was also no change in the AMPA EPSC decay time (wild type, 19.4 ± 4 ms; knockout, 21.9 ± 4.6 ms) or GABA inhibitory postsynaptic current (IPSC) decay time (wild type, 76 ± 4.9 ms; knockout, 58.8 ± 7 ms). In addition, we found no change in stimulus intensity versus fEPSP (field excitatory postsynaptic potential) slope or fiber volley amplitude (fig. S5, M and N) and no change in paired pulse ratio (fig. S5O), suggesting that Syt3 does not affect the number of synaptic inputs from CA3 onto CA1 neurons or short-term presynaptic plasticity.

Syt3 promotes LTD and decay of LTP

LTD—which requires activity-dependent endocytosis of AMPA receptors—was abolished in Syt3 knockouts (Fig. 4A), which is consistent with defective activity-dependent AMPA receptor endocytosis in the absence of Syt3. In wild-type slices, application of the GluA2-3Y peptide, which disrupts Syt3 binding to the GluA2 cytoplasmic tail, mimicked the Syt3 phenotype and abolished LTD (Fig. 4A) (*8*, *11*, *35*).

The decay of LTP induced by means of a 1XTET stimulation (a single tetanus of 16 pulses at 100 Hz) also depends on receptor internalization (*13*). LTP induced by means of a 1XTET stimulus decayed within 1 hour in wild-type slices (*36*) but was reinforced and remained potentiated in Syt3 knockouts (Fig. 4B); this form of LTP was NMDA receptor–dependent in both wild-type and Syt3 knockout slices (fig. S6, A and B). The GluA2-3Y peptide again mimicked the Syt3 knockout phenotype and reinforced decaying LTP (Fig. 4C). This reinforced decaying LTP was insensitive to ZIP (PKMζ inhibitory peptide) (Fig. 4C), which blocks the activity of atypical protein kinases and has the unusual property of reversing LTP after induction, through endocytosis of AMPA receptors (*12*, *13*, *37*, *38*). Reinforced decaying LTP in Syt3 knockouts was similarly ZIP-insensitive (Fig. 4D). The GluA2-3Y peptide had no effect on the reinforced decaying LTP in Syt3 knockouts, confirming that Syt3 decays LTP by acting on the GluA2-3Y region (Fig. 4D).

Nondecaying LTP, induced by means of 3XTET stimulation (three tetanizing trains of 100 pulses at 100 Hz), was unchanged in Syt3 knockout hippocampal slices compared with wild-type slices (Fig. 4E). However, ZIP promoted decay of 3XTET-induced LTP in wild-type slices but not in Syt3 knockout slices (Fig. 4F), further indicating a defect in activity-dependent receptor internalization in Syt3 knockouts. Because ZIP had no effect on LTP in Syt3 knockout slices, it did not appear to cause excitotoxicity or neural silencing (*39*, *40*). Analysis of stimulation frequency–potentiation dependence revealed increased potentiation in Syt3 knockouts compared with wild-type slices (Fig. 4G).

To test whether calcium-sensing by postsynaptic Syt3 is important for receptor internalization in these plasticity paradigms, we injected wild-type or calcium-binding–deficient mutant Syt3 AAV1/2 postsynaptically into the dorsal CA1 region of the hippocampus of mice in which Syt3 had been knocked out (Syt3 knockout mice) (Fig. 4H). We found that LTD (Fig. 4I), decaying 1XTET-induced LTP (Fig. 4J), and ZIP-mediated decay of 3XTET LTP (Fig. 4K) were rescued by expression of wild-type Syt3 but not calcium-binding–deficient Syt3.

Syt3 knockout mice learn normally but have impaired forgetting

Because Syt3 knockout mice had normal LTP but lacked LTD, we hypothesized that they would learn normally but have deficits in forgetting. To test this, we used the water maze spatial memory task that involves the CA1 hippocampal subregion, in which mice learn to navigate to a hidden platform position over sequential days of training using visual cues. Syt3 knockout mice showed no difference in anxiety or hyperactivity (fig. S7, A to C) but had a 15% decrease in body weight and faster swim speed compared with those of wild-type mice (fig. S7, D and E). We therefore plotted proximity to the platform in addition to the traditional escape latency parameter to control for possible effects of swim speed. The maximum average proximity difference—between closest (after training of all mice to a platform position) and farthest possible proximity (by using the same data but calculating proximity to a platform in the opposite quadrant)—was 12.5 cm. Syt3 knockout and wild-type mice learned the position of the hidden platform equally well; there was no significant difference in proximity to the platform (Fig. 5A) or escape latency (fig. S7F) during training. When the platform was removed in probe tests after training, to test how well the mice have learned the platform position, the percentage of time spent in the target quadrant was well above chance level for both Syt3 knockout and wild-type mice (Fig. 5B), and proximity to the platform position (Fig. 5C) and platform position crossings (Fig. 5D) were similar. Syt3 knockout mice in cohort 1 (of two cohorts tested) had significantly lower proximities and more platform crossings in the first probe test compared with those of wild-type mice but no difference in the second probe test. Thus, Syt3 knockout mice learned the task as well or slightly faster than did wild-type mice.

We observed an indication of a lack of forgetting in the second probe test after learning. Syt3 knockout mice exhibited a lack of "within-trial" extinction. Wild-type mice showed maximal searching (proximity to the platform) in the first 10 to 20 s of the probe test and then gradually shifted to a dispersed search pattern of other regions of the pool (*41*), whereas Syt3 knockout mice continued to persevere to the platform position even near the end of the trial (Fig. 5E). When the platform was shifted to the opposite quadrant in reversal training, Syt3 knockout mice learned the new platform position as well as did wild-type mice in the probe test (probe test 3) (Fig. 5, B, C, and D) but continued to persevere to the original platform position during reversal training (fig. S7G) and in the probe test after reversal (Fig. 5F), exhibiting a lack of forgetting of the previous platform position.

In a fourth cohort, we extended the training days after reversal (fig. S7H). Syt3 knockout mice persevered to the previous platform position significantly more than did wild-type mice, even after 7 days of reversal training (Fig. 5G). Injection of Syt3 AAV1/2 specifically into the dorsal CA1 (postsynaptic) region of the hippocampus of Syt3 knockout mice rescued this perseverence phenotype, compared with Syt3 knockout or wild-type mice injected with control GFP AAV1/2 (Fig. 5G).

To test whether the lack of forgetting exhibited by Syt3 knockouts is due to defective AMPA receptor internalization, we trained wild-type and Syt3 knockout mice to learn a platform position in the water maze, during habituation to daily saline intraperitoneal injections (fig. S7I). We then injected the Tat-GluA2-3Y peptide (5 μmol/kg, intraperitoneally)—which disrupts Syt3:GluA2 binding and blocks AMPA receptor internalization (*11*–*13*, *35*)—1 hour before the probe test after training to the initial platform position, and then daily, 1 hour before reversal training to a new platform position in the opposite quadrant. In the probe test after training to the initial platform position, peptide-injected wild-type and Syt3 knockout mice showed a similar lack of within-trial extinction and continued to persevere to the platform position, whereas saline-injected wild-type mice shifted to a dispersed search pattern near the end of the trial (Fig. 5H and fig. S7J). Similarly, in probe tests after reversal training to a new platform position, wild-type mice injected with the Tat-GluA2-3Y peptide persevered to the original platform position significantly more than did saline-injected wild-type mice [$P = 0.042$; one-way analysis of variance (ANOVA), Bonferroni's correction] or uninjected wild-type mice in previous cohorts ($P = 0.039$) and to a similar extent as did Tat-GluA2-3Y peptide–injected Syt3 knockout mice ($P = 0.096$) or uninjected Syt3 knockout mice in previous cohorts ($P = 0.105$) (Fig. 5I). Thus, Tat-GluA2-3Y peptide injection mimics the Syt3 knockout phenotype. There was no difference in perseverence between Tat-GluA2-3Y–injected and uninjected Syt3 knockouts in previous cohorts ($P = 0.184$), indicating that the effect of Tat-GluA2-3Y peptide injection is occluded in Syt3 knockout mice.

To further test whether the lack of forgetting phenotype of Syt3 knockouts is due to a lack of receptor internalization via Syt3:GluA2 interaction, we tested spatial memory in the Barnes maze, in which mice learn to navigate to 1 of 20 holes around the perimeter of a circular platform leading to an escape cage, using visual cues. Time spent in the target hole area during training and

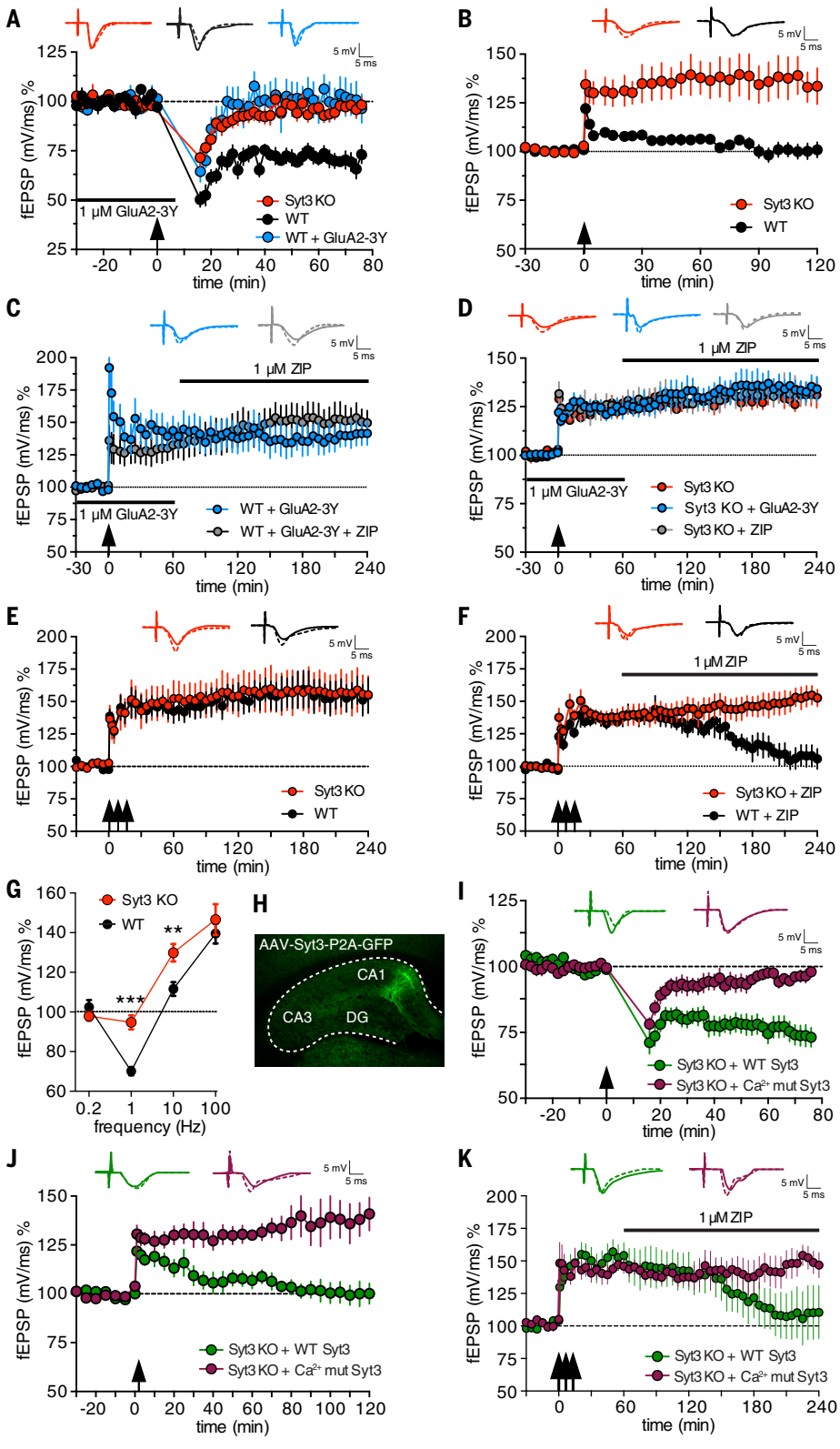

Fig. 4. LTD and decay of LTP is abolished in Syt3 knockouts. (**A**) LTD is abolished in Syt3 KO, and Tat-GluA2-3Y peptide treated WT hippocampal slices (*n*; slices/mice, 12/8 Syt3 KO, 8/6 WT, and 8/5 WT + Tat-GluA2-3Y); ***$P < 0.001$ for Syt3 KO/WT; **$P < 0.05$ for WT +GluA2-3Y/WT. (**B**) 1XTET-induced LTP is reinforced in Syt3 KO slices compared with WT ($n = 10/7$ Syt3 KO, 10/10 WT); **$P < 0.05$. (**C**) 1XTET-induced LTP in WT slices treated with the Tat-GluA2-3Y peptide is reinforced and ZIP-insensitive ($n = 7/7$). (**D**) Reinforced 1XTET-induced LTP in Syt3 KOs is unchanged by the Tat-GluA2-3Y peptide and is ZIP-insensitive ($n = 6/6$ Syt3 KO, 7/7 Syt3 KO + GluA2-3Y peptide, 7/7 Syt3 KO + ZIP). (**E**) 3XTET-induced LTP is unchanged in Syt3 KO compared with WT ($n = 6/6$). (**F**) 3XTET-induced LTP in Syt3 KOs is ZIP-insensitive ($n = 6/6$); **$P < 0.01$. (**G**) fEPSP changes in Syt3 KO and WT slices induced by different stimulation frequencies, recorded 30 min after stimulation [Syt3 KO/WT, $n = 9/12$ (0.2 Hz), 9/12 (1 Hz), 12/7 (10 Hz), and 14/14 (100 Hz)]. (**H**) GFP fluorescence in a hippocampal slice from a mouse injected with AAV1/2 Syt3-P2A-GFP in the dorsal CA1 region. (**I**) LTD in Syt3 KOs is rescued by hippocampal CA1 AAV1/2 injection of WT Syt3 ($n = 13/11$) but not calcium-binding deficient Syt3 (Ca^{2+} mut) ($n = 8/6$); **$P < 0.01$. (**J**) Decay of 1XTET-induced LTP in Syt3 KOs is rescued by WT ($n = 8/6$) but not Ca^{2+} mut Syt3 ($n = 7/6$ mice); **$P<0.01$. (**K**) ZIP-mediated decay of 3XTET-induced LTP in Syt3 KOs is rescued by WT ($n = 5/5$) but not Ca^{2+} mut Syt3 ($n = 6/6$); *$P < 0.05$; Mann-Whitney U test or Kruskal-Wallis test with Dunn's test for multiple comparisons; *n* = slices/mice.

in subsequent probe tests gives a readout of spatial memory. We tested four groups simultaneously: wild-type mice and Syt3 knockout mice, injected with saline or GluA2-3Y peptide, during "reversal" training to a new hole after initial learning of an original hole position. We predicted that (i) Syt3 knockout mice would exhibit a lack of forgetting—persevere more to the original hole after reversal as compared with wild-type; (ii) disruption of Syt3:GluA2 interaction through injection of the GluA2-3Y peptide in wild-type mice would mimic the lack of forgetting phenotype of Syt3 knockouts; and (iii) injection of the GluA2-3Y peptide in Syt3 knockout mice would have no effect on their lack of forgetting.

In initial training, all four groups (injected intraperitoneally daily with saline only, 1 hour before training) learned the target hole equally

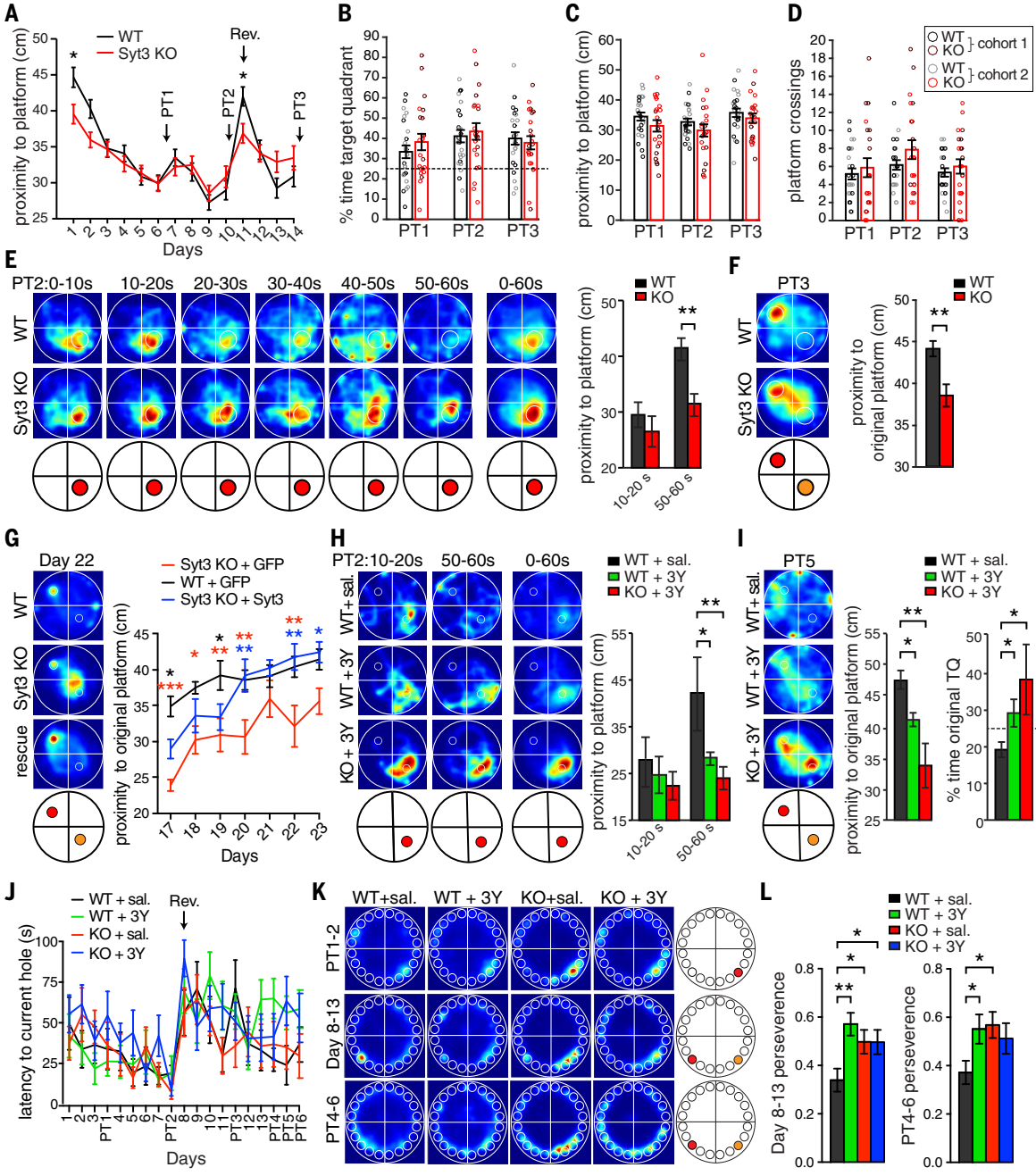

Fig. 5. Syt3 knockout mice learn as well as wild-type mice but have impaired forgetting. (**A**) Syt3 KO and WT mice had similar proximity to the platform during training (genotype effect, $P = 0.1052$; two-way ANOVA, Bonferroni's test) and in probe tests exhibited similar percent of time in (**B**) target quadrant, (**C**) proximity to platform, and (**D**) platform crossings. KOs in cohort 1 had lower proximities than those of WT in probe tests ($P = 0.027$; Student's t test). (**E**) Syt3 KO mice lack within-trial-extinction in time-binned average occupancy plots of all mice and proximity to the platform position (red in schematics) in probe test 2. (**F**) Syt3 KO mice persevere to the previous platform position (orange) in the probe test after reversal training (to the red platform position) ($n = 9/13$ Syt3 KO and 10/14 WT mice for cohort 1/cohort 2); Student's t test, Welch's correction in (B), (C), (E), and (F) and Mann-Whitney U test in (D). (**G**) Expression of Syt3 in the hippocampal CA1 region rescues the perseverence phenotype of Syt3 KOs in training after reversal; two-way ANOVA, Tukey's test. Black, red, and blue asterisks are significance between WT+GFP/Syt3 KO+Syt3, Syt3 KO+GFP/WT+GFP, and Syt3 KO+GFP/Syt3 KO+Syt3, respectively ($n = 10$ Syt3 KO+Syt3, 7 Syt3 KO+GFP, and 15 WT+GFP). (**H**) Injection of the Tat-GluA2-3Y peptide mimics the lack of within-trial-extinction in probe test 2 after initial training, and (**I**) perseverence to the previous platform position in probe tests after reversal training, exhibited by Syt3 knockouts ($n = 8$ WT saline, 7 WT+3Y, and 10 Syt3 KO+3Y); one-way ANOVA, Bonferroni's correction. (**J**) All mice learned (decreased latency to) the escape hole in the Barnes maze equally well during training (two-way ANOVA, Tukey's test) and (**K**) (top) in probe tests 1 and 2 after training. (Middle) In reversal training and (bottom) probe tests 4 to 6 after reversal training, WT saline mice learned the new hole position (red), but WT+3Y, KO saline, and KO+3Y mice persevered to the previous hole position (orange). (**L**) WT+3Y, KO saline, and KO+3Y mice had a higher perseverence ratio [time spent exploring original hole (orange) divided by total time spent exploring original and reversal (red) holes] as compared with that of WT saline mice ($n = 10$ WT saline, 11 WT+3Y, 11 Syt3 KO saline, 12 Syt3 KO+3Y; $P = 0.060$ for WT saline/Syt3 KO+3Y in probe tests 4 to 6); one-way ANOVA, Bonferroni's correction. All occupancy plots show average search path densities across all mice in a group.

well (Fig. 5J) and spent the majority of their time exploring the target hole region in probe tests (Fig. 5K, top). Beginning on the day of probe test 2 and during reversal training, in which the target hole was positioned in a different quadrant, mice were injected with saline or GluA2-3Y peptide 1 hour before training each day. Saline-injected Syt3 knockout mice and GluA2-3Y-injected wild-type and Syt3 knockout mice all showed a similar increased perseverence to the original hole region as compared with wild-type saline-injected mice throughout reversal training (Fig. 5K, middle) and in probe tests after reversal training (Fig. 5, K, bottom, and L), which is in agreement with our prediction.

Syt3 knockouts have impaired working memory owing to lack of forgetting

To further test deficits in forgetting exhibited by Syt3 knockout mice, we examined working memory in the delayed matching to place (DMP) water maze task, in which the platform position is moved to a new position each day (*42*). Each day, the mice have four trials to learn the new platform position and forget the previous platform position. We first trained the mice to a visible platform for 3 consecutive days, in which Syt3 knockout and wild-type mice performed equally well (fig. S8A). Because swimming speed of Syt3 knockout mice was again faster than that

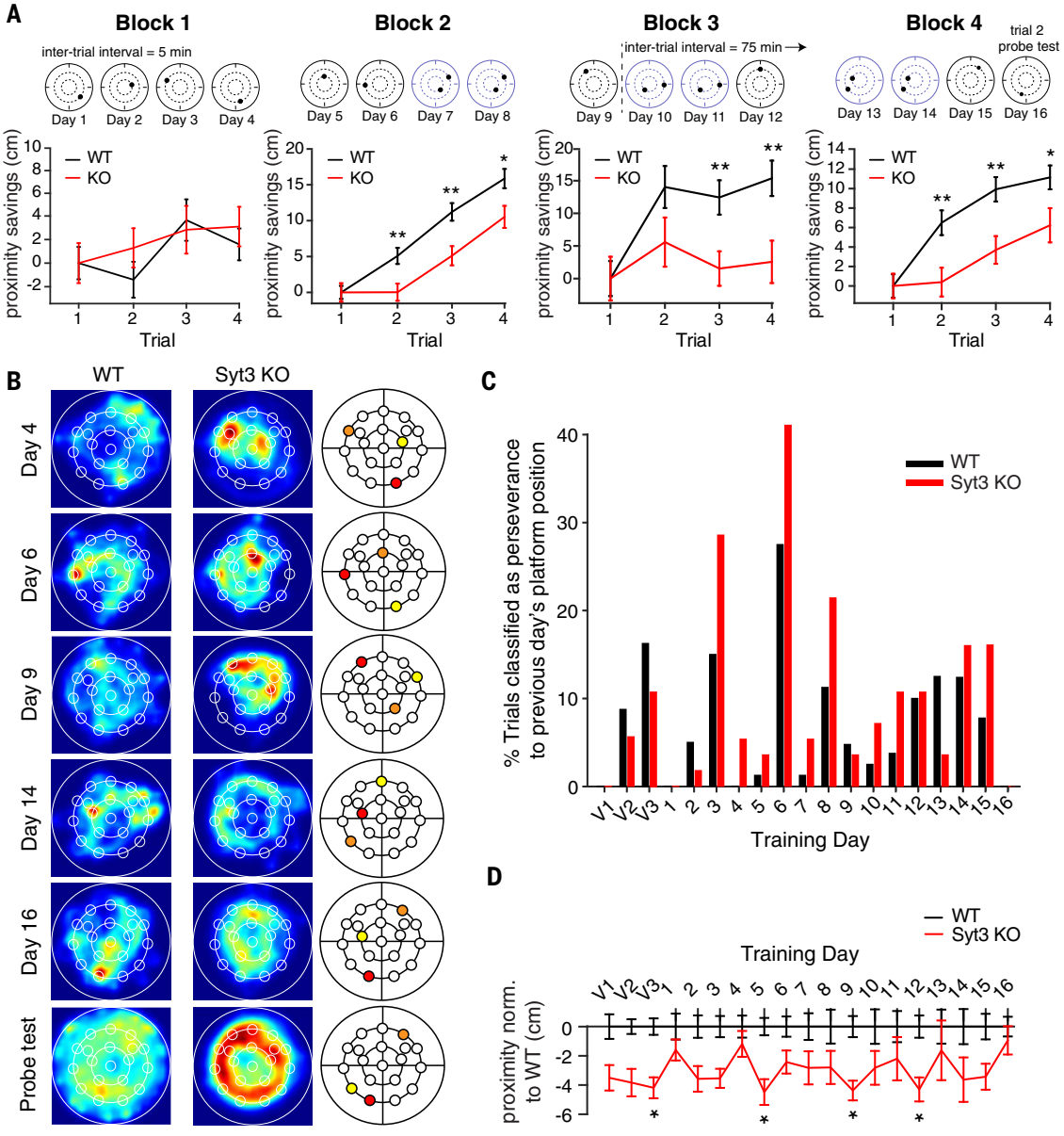

Fig. 6. Syt3 knockout mice show deficits in the delayed matching to place task because of impaired forgetting. (**A**) WT mice had a closer proximity to the platform in trials 2 to 4 relative to trial 1 (higher proximity savings) as compared with that of Syt3 KO mice, indicating that Syt3 KOs had deficits in finding the platform when it appeared in a new position each day. Hidden platform positions presented each day are indicated above the graphs. Blue-outlined mazes indicate counter-balancing, in which half the cohort is trained to one of the positions and the other half is trained to the other position, to avoid biased search of inner- or outer-platform positions (n = 14 Syt3 KO and 20 WT mice); Student's t test. (**B**) Occupancy plots of individual trials averaged across all mice on training days, and in the probe test after training, reveal impaired forgetting in Syt3 KO mice—higher perseverence to previous days' platform positions as compared with that of WT. In maze schematics, the current day's platform is red, the previous day's is orange, and the platform position 2 days previous is yellow. (**C**) Syt3 KOs have significantly more perseverence trials compared with those of WT in strategy analysis (P = 0.0383; unpaired t test, Welch's correction). (**D**) In the probe test on day 16, Syt3 KO mice persevere more (have closer proximity as compared with WT) to all previous positions. V1, V2, and V3 indicate visible platform training days; two-way ANOVA for genotype effect, $P < 0.0001$; Bonferroni's test, $^*P < 0.05$.

of wild-type mice (fig. S8B), we quantified proximity savings in hidden platform training (Fig. 6A). In the first 4 days of training, mice became accustomed to the task. In the second 4-day block, mice had learned the task, and wild-type mice performed significantly better than Syt3 knockouts. In the third block, from day 10 onward, the intertrial interval between trial 1 and trial 2 was increased from 5 to 75 min, and wild-type mice continued to perform better than Syt3 knockout mice; this difference was most pronounced in the fourth 4-day block of training (Fig. 6A). Quantitation of escape latency savings (fig. S8D) and path savings (fig. S8E) yielded similar results. To test whether the poor performance of Syt3 knockouts was due to difficulty forgetting previous platform positions, we examined perseverance to previous positions. Occupancy plots indicated that Syt3 knockouts indeed persevered to previous platform positions more than did wild-type mice throughout training and sampled most previous platform positions in the probe test, whereas wild-type mice adopted a more random search pattern (Fig. 6B). Syt3 knockout mice had significantly more trials classified as perseverence (*43*) to the previous day's platform position as compared with wild-type mice across all days of training (P = 0.0383, unpaired t test, Welch's correction) (Fig. 6C). Neither Syt3 knockout nor wild-type mice exhibited chaining (*43*), a nonspatial search strategy for platform positions at two fixed distances from the wall (fig. S8C). Syt3 knockout mice also had a significantly closer proximity to all previous platform positions in the probe test at the end of the 16-day training period, compared with that of wild-type mice (Fig. 6D).

Discussion

We found that activity-dependent AMPA receptor internalization, LTD, decay of LTP, and forgetting of spatial memories requires Syt3. In rescue experiments, calcium-sensing by postsynaptic Syt3 was required for LTD and the decay of LTP. The GluA2-3Y peptide competitively inhibited Syt3 binding to the 3Y region of the GluA2 receptor tail. Introduction of this peptide in a wild-type background mimicked the Syt3 knockout phenotypes of lack of activity-dependent AMPA receptor internalization, LTD, decay of LTP, and forgetting. Effects of the peptide were occluded in Syt3 knockout mice, implicating Syt3 in a GluA2-3Y–dependent mechanism of AMPA receptor internalization.

Our data give rise to a model in which Syt3 at postsynaptic endocytic zones is bound to AP-2 and BRAG2 in the absence of calcium. GluA2 could then accumulate at endocytic zones by binding Syt3 in response to increased calcium during neuronal activity. This would potentially bring GluA2 into close proximity to BRAG2, where a transient interaction could activate BRAG2 and Arf6, and promote endocytosis of receptors via clathrin and AP-2 (*10*, *32*). PICK1 is also important for AMPA receptor endocytosis, raising the question of the interplay of Syt3 and PICK1. Two possible mechanisms are conceivable. PICK1 could sequester receptors internally after endocytosis (*44*) and act downstream of Syt3. Alternatively, PICK1 could transiently bind GluA2 and then AP-2 after stimulation, to cluster AMPA receptors at endocytic zones and promote their subsequent internalization (*45*). Thus, it is also possible that PICK1 acts upstream of or in concert with Syt3 to bring GluA2 to endocytic zones.

Blockade of postsynaptic expression of Syt1/Syt7 was recently reported to abolish LTP but have no effect on LTD (*18*). Thus, distinct Syts may insert and remove receptors from the postsynaptic membrane to mediate LTP and LTD, respectively. Syts may regulate both exo- and endocytosis (*46*) but be predisposed to one or the other depending on their calcium affinity. Endocytosis occurs on slower time scales than does exocytosis. As calcium concentration declines, high-affinity Syts such as Syt3 (*22*) may remain active, whereas low-affinity Syts such as Syt1 inactivate. Alternatively, Syts predisposed to endocytosis may interact with protein complexes that extend association with Ca^{2+} or bind proteins in resting conditions that are released upon Ca^{2+} binding to cause endocytosis.

Although the ability to remember is often regarded as the most important aspect of memory, forgetting is equally important. Deficits in forgetting can have severe consequences and lead to posttraumatic stress disorder, for example. Our data identify Syt3 as a molecule important for a forgetting mechanism by which AMPA receptors are internalized to promote LTD and decay of LTP.

Materials and methods

Animals

Use of mice for experimentation was approved and performed according to the specifications of the Institutional Animal Care and Ethics Committees of Göttingen University (T10.31), and German animal welfare laws. Animal sample size was estimated by experimental literature and power analysis (G* Power version 3.1) to reduce animal number where possible while maintaining statistical power. The Syt3 and Syt6 knock-out and Syt5 and Syt10 knock-in quadruple targeted mutation mice (B6;129-Syt6^{tm1Sud} Syt5^{tm1Sud} Syt3^{tm1Sud} Syt10^{tm1Sud}/J, stock no. 008413) were obtained from The Jackson Laboratory (www.jax.org/strain/008413). These mice were then crossed with Black6/J mice, obtained from Charles River, to isolate mice with homozygous knock-out alleles of Syt3 but WT alleles of Syt5, Syt6 and Syt10. The genotypes of all breeder pairs and mice used for behavioral experiments were confirmed by PCR.

Dissociated hippocampal culture and neuronal transfection

Rat hippocampi were isolated from E18-19 Wistar rats as described previously (*47*). Hippocampi were treated with trypsin (Sigma) for 20 min at 37°C, triturated to dissociate cells, plated at 40,000 cells/cm^2 on poly-D-lysine (Sigma)–coated coverslips (Carolina Biologicals), and cultured in Neurobasal medium supplemented with 2% B-27 and 2 mM Glutamax (Gibco/Invitrogen). Cultures were fixed at 12 to 18 DIV with 4% paraformaldehyde and immunostained with primary antibodies, followed by secondary labeling with Alexa dyes for confocal imaging.

Hippocampi from P0 mouse brains were dissected in ice cold dissection medium (HBSS (Gibco), 20 mM HEPES (Gibco), 1.5 mM $CaCl_2$, 10 mM $MgCl_2$, pH adjusted to 7.4 with NaOH) and then incubated in a papain digestion solution (dissection medium, 0.2 mg/ml L-Cysteine, 0.5 mM NaEDTA, 1 mM $CaCl_2$, 3 mM NaOH, 1% Papain equilibriated in 37°C and 5% CO_2 + 0.1 mg/ml DNAseI) for 30 min at 37°C and 5% CO_2. Papain was inactivated with serum medium [DMEM, 2 mM Glutamax, 5% FBS, 1X Mito$^+$ supplements (VWR), 0.5X MEM vitamins (Gibco)] + 2.5 mg/ml BSA + 0.1 mg/ml DNAseI, followed by 3 washes with serum medium. After trituration in serum medium, the cell suspension was centrifuged for 5 min at 500 × g at room temperature. The cell pellet was resuspended in plating medium (Neurobasal medium, 100 U/ml Pen/Strep, 2% B27, 0.049 mM L-aspartate, 0.05 mM L-glutamate, 2 mM Glutamax, 10% serum medium). Cells were plated at 60,000 cells/cm^2 on 12 mm diameter acid-etched glass coverslips coated with 0.04% Polyethyleneimine (PEI; Sigma). Glial growth was blocked on DIV4 with 200 µM FUDR. 50% conditioned medium was replaced with feeding medium (Neurobasal, 2 mM Glutamax, 100 U/ml Pen/Strep, 2% B-27) on DIV7.

For transfection of neurons on 12 mm coverslips in 24-well plates, the culture medium from each well was exchanged with 400 µl Neurobasal medium; the original culture medium was stored at 37°C and 5% CO_2. 1 µg DNA/50 µl Neurobasal medium and 1 µl Lipofectamine 2000 (Gibco)/50 µl Neurobasal medium were incubated separately for 5 min, mixed, and incubated for 20 additional min, before adding the mixture to neurons in a well. Following incubation for 2 hours, neurons were washed once with Neurobasal, and conditioned media was replaced.

HEK cell culture, transfection, immunostaining, and Western blots for Syt3 knockdown validation

Human embryonic kidney (HEK) 293 cells (purchased from American Type Culture Collection CRL-3216; not tested for mycoplasma) cultured in DMEM supplemented with 10% FBS on 10 cm dishes were transfected at 60 to 80% confluence using the calcium-phosphate method: 20 µg plasmid DNA in 360 µl dH_2O was mixed with 40 µl 2.5 M $CaCl_2$, followed by addition of an equal volume (400 µl) of transfection buffer (280 mM NaCl, 1.5 mM Na_2HPO_4, 50 mM HEPES, pH 7.05). This mixture was incubated at room temperature for 20 min and 800 µl added per dish. 24 to 48 hours later cells were harvested for Western blots in lysis buffer (50 mM Tris-HCl pH 7.5, 150 mM NaCl, 2 mM EDTA, 0.5% NP40, and protease inhibitors). For immunostaining, HEK cells growing on 12 mm coverslips were transfected with Lipofectamine 2000 (Invitrogen) by incubating 1 µg DNA/50 µl medium and 1 µl Lipofectamine 2000/50 µl medium separately for 5 min, mixing the two solutions together, and

then incubating for an additional 20 min, before adding the mixture to wells of a 24-well plate.

Immunohistochemistry

Acute hippocampal slices were prepared from 8-week-old mice anesthetized with isoflurane and decapitated. The hippocampus was removed and 200 μm thick slices were cut transversely using a tissue chopper (Stoelting) in ice-cold artificial cerebrospinal fluid (ACSF) containing, in mM 124 NaCl, 4.9 KCl, 1.2 KH_2PO_4, 2 $MgSO_4$, 2 $CaCl_2$, 24.6 $NaHCO_3$, and 10 D-glucose (saturated with 95% O_2 and 5% CO_2, pH 7.4, ~305 mOsm). Slices were fixed in 4% paraformaldehyde in PBS for 30 min and washed 3 X 20 min in PBS. After washing, slices were incubated in antibody buffer (2% donkey serum, 0.1% Triton X-100 and 0.05% NaN_3 in PBS) for 30 min at room temperature. Then slices were incubated with primary antibodies in antibody buffer overnight at 4°C. Slices were then washed with PBS 3 X 20 min and incubated with fluorescently tagged secondary antibodies for 2 hours at room temperature. Slices were washed 3 X 20 min in PBS and mounted on microscope slides with Fluoromount-G (Sigma) and sealed with nail polish. Images were collected using 10X air and 40X oil immersion objectives on a Zeiss A1 laser scanning confocal microscope with Zen software (Carl Zeiss). Digital images were processed using Adobe Photoshop software.

Antibodies and expression constructs

Antibodies used including species and catalog number were rabbit Syt3 105133 (Synaptic Systems) and mouse Syt3 N278/19 (NeuroMab), chick MAP2 C-1382-50 (Biosensis), rabbit GFP ab290 (Abcam), mouse Synaptophysin (Syp) 101011, rabbit Synaptobrevin2 (Syb2) 104202, mouse Syt1 105101, mouse SNAP25 111011, guinea pig Piccolo 142104, guinea pig Homer 160004, guinea pig Beta3-tubulin 302304, rabbit VGluT1 135303, mouse VGAT 131011, mouse Rab-GDI 130011, mouse Gephyrin 147011, rabbit GluA1 182003, mouse GluA2 182111, rabbit GRIP 151003 (Synaptic Systems), mouse $GABA_AR\alpha1$ 75136 (NeuroMab), rabbit GluA3 17311 (Epitomics), mouse PSD95 MA1-045 (Thermo Scientific), rabbit GluA1 PC246 (Calbiochem), mouse GluA2 MAB397, rabbit GluN1 AB9864, mouse GluN2A MAB5216 (Millipore), rabbit PICK1 PA1073 (Thermo Scientific), mouse Synapsin (Syn), mouse Rab3a, mouse Syntaxin1A, rabbit EEA1 (provided by Reinhard Jahn, Max Planck Institute for Biophysical Chemistry, Goettingen, Germany), rabbit Neurexin (Nrx), rabbit Neuroligin (Nlg) (provided by Nils Brose, Max Planck Institute of Experimental Medicine, Goettingen, Germany), mouse AP-2 (provided by Pietro De Camilli, Yale School of Medicine, New Haven, CT, USA), and rabbit BRAG2 (*10*) (provided by Hans-Christian Kornau, Charité University of Medicine, Berlin, Germany). Mammalian expression constructs used were pHluorin-Syt3, as previously described (*23*). GFP-Syt3 and mCherry-Syt3 were subcloned by replacing the pHluorin in pHluorin-Syt3 with GFP or mCherry, respectively. Homer-GFP, Homer-myc, and Clathrin light chain (CLC)-DsRed constructs were provided by Daniel Choquet (*30*) (University of Bordeaux). The calcium-binding deficient mutant of Syt3 was generated by Genscript by mutagenesis of D386, 388N and D520, 522 N, corresponding to the calcium-binding sites of syt1: D230, 232 N and D363, 365 N (*48*). Syt3 shRNA knockdown constructs, transfected in equal amounts, were KD1; TGCTGTTGACAGTGAGCGACAAGCTCATCGGTCAGATCAATAGTGAAGCCACAGATGTATTGATCTGACCGATGAGCTTGGTGCCTACTGCCTCGGA, KD2; TGCTGTTGACAGTGAGCGCAGGTGTCAAGAGTTCAACGAATAGTGAAGCCACAGATGTATTCGTTGAACTCTTGACACCTATGCCTACTGCCTCGGA and KD3; TGCTGTGACAGTGAGCCAGGATTGTCAGAGAAAGAGAATAGTGAAGCCACAGATGTATTCTCTTTCTCTGACAATCCTTTGCCTACTGCCTCGGA in a pGIPZ vector co-expressing turboGFP (Thermo Scientific Openbiosystems).

Receptor internalization assays

Neurons were labeled with primary extracellular antibodies against GluA1 (rabbit PC246 Calbiochem) or GluA2 (mouse MAB397 Millipore) in medium for 15 min at 37°C and 5% CO_2, washed for 2 min in medium, and then stimulated with 100 μM AMPA or NMDA for 2 min, followed by incubation in conditioned medium for an additional 8 min at 37°C and 5% CO_2, before fixing cells with 4% paraformaldehyde. Surface receptors were labeled with Alexa 647 secondary antibodies, then cells were permeabilized and internal receptors labeled with Alexa 546 secondary antibodies. The internalization index was calculated as the ratio of internal to surface receptor fluorescence. Cultures in which control conditions did not show an increase in internalization following stimulation were excluded from analysis.

pHluorin imaging

Neurons were transferred to a live imaging chamber (Warner Instruments) containing bath saline solution (140 mM NaCl, 5 mM KCl, 2 mM $CaCl_2$, 2 mM $MgCl_2$, 5.5 mM glucose, 20 mM HEPES, 1 μM TTX, pH = 7.3). Transfected cells were selected, and images acquired at 1 s intervals and 500 ms exposure times, with 484/20nm excitation and 517/20-nm emission filters, on a Zeiss Axio Observer inverted microscope with a Photometric Evolve EMCCD camera, and Lambda DG-4 fast-switching light source interfaced with Metamorph software. A baseline of at least 30 images was collected before addition of high potassium buffer (100 mM NaCl, 45 mM KCl, 2 mM $CaCl_2$, 2 mM $MgCl_2$, 5.5 mM glucose, 20 mM HEPES, 1 μM TTX, pH = 7.3), 100 μM AMPA, 100 μM NMDA, or field stimulation to depolarize neurons. For AMPA stimulation, 50 μM AP5 was included in the bath solution to block NMDA receptors; for NMDA stimulation, 20 μM CNQX was included to block AMPA receptors. Dendritic puncta were selected using Metamorph software (Molecular Devices) and fluorescence intensity normalized to baseline was plotted versus time.

Subcellular fractionation from whole brain

Rat brains were homogenized in ice-cold homogenization buffer (320 mM sucrose, 4 mM HEPES, pH 7.4 with NaOH) with 10 strokes at 900 rpm. Samples were then centrifuged at 1000 × g for 10 min. The supernatant (S1) was collected; the resulting pellet (P1) contains large cell fragments and nuclei. S1 was then centrifuged at 15,000 × g for 15 min. The supernatant (S2) contains soluble proteins and the pellet (P2) contains synaptosomes. The pellet was then carefully resuspended in 1 ml homogenization buffer, 9 ml ice-cold ddH_20 was added and three strokes at 2,000 rpm were performed. 50 μl 1M HEPES and protease inhibitors were added. The lysate was centrifuged at 17,000 × g for 25 min to separate synaptosomal membranes (LP2) from synaptosomal cytosol (LS2). The LP2 pellet was resuspended in 6 ml 40 mM sucrose and layered over a continuous sucrose gradient from 50 mM to 800 mM. The sucrose cushion was then centrifuged at 28,000 rpm for 2 hours. Following centrifugation, the region between approximately 200 mM and 400 mM sucrose was collected and separated by chromatography on controlled-pore glass beads (CPG column) and run overnight. The first peak (PI) contained larger membrane fragments and SVs were found in the second peak.

Immuno-organelle isolation of synaptic vesicles

Mouse monoclonal antibodies directed against Syb2 and Syt1 were coupled to Protein G magnetic Dynabeads (Invitrogen) in PBS for 2 hours at 4°C. Antibody-coated beads were added to whole brain S1 fractions and incubated overnight at 4°C. Magnetic beads were separated from immuno-depleted supernatant and washed 3 times with PBS. Bound vesicles were eluted in sample buffer and analyzed by SDS–polyacrylamide gel electrophoresis (SDS-PAGE) and immunoblotting.

Syt3 pulldowns

Recombinant His-tagged Syt3 C2AB (provided by Edwin Chapman, University of Wisconsin, Madison) was expressed in *E. coli* and purified as previously described (*49*). Recombinant Syt3 was incubated with solubilized rat brain homogenate for 2 hours at 4°C. After incubation, Ni-beads were added and incubated for an additional 2 hours at 4°C. The mixture was then poured into a MT column from Biorad and washed 3 X with wash buffer (20 mM Tris pH 7.4, 500 mM NaCl, 20 mM imidazole). Proteins bound to recombinant Syt3 in the column were eluted with elution buffer (20 mM Tris pH 7.4, 500 mM NaCl, 400 mM imidazole). For experiments testing inhibition of Syt3:GluA2 binding, 1 μM Tat-GluA2-3Y peptide (sequence $YGRKKRRQRRR\text{-}_{869}YKEGYNVYG_{877}$, provided by Yu-Tian Wang, University of British Columbia, Vancouver, Canada) was pre-incubated with brain homogenate overnight prior to incubation with recombinant Syt3 and Ni-beads. Eluted proteins were loaded onto SDS-PAGE gels and analyzed by Western blot.

Synaptosome trypsin cleavage assay

Synaptosomes were prepared and treated with trypsin as described previously (*26*). Purified synaptosomes were centrifuged for 3 min at 8700 × g,

4°C. The pellet was resuspended in 320 mM sucrose, 5 mM HEPES, pH 8. For trypsin cleavage, a 0.1 mg/ml trypsin stock solution was added to yield a final protein-protease ratio of 100:1. Synaptosomes were incubated for 10, 20, 30, 60, or 90 min at 30°C with gentle agitation. This mixture was then centrifuged for 3 min at 8700 × g, and the resulting pellet resuspended in sucrose buffer containing 400 μM Pefabloc (Roche) to stop trypsin cleavage activity. Samples were then analyzed by SDS-PAGE and immunoblotting.

AAV preparation and hippocampal injections

AAV ESYN-GFP-P2A-Syt3 or calcium-binding deficient mutant Syt3 (D386, 388N, and D520, 522N) constructs were synthesized and subcloned by Genscript, and AAV1/2 viral particles prepared by transfecting 10 cm dishes of 70-80% confluent HEK293 cells with 12.5 μg of viral construct containing Syt3 or calcium-binding deficient mutant Syt3, with 25 μg pFdelta6, 6.25 μg pRV1 and 6.25 μg pH21 helper plasmids using calcium phosphate. Cell media was replaced after 6 hours and cells incubated for 48 hours prior to virus harvesting. Viral particles were released by adding 10% sodium deoxycholate and benzonase (Sigma-Aldrich), and purified in an Optiprep (Sigma-Aldrich) step gradient by ultracentrifugation for 90 min. The pure viral fraction was concentrated to approximately 500 μl through a 0.22 μm Amicon Ultra unit (Millipore/Merck), aliquoted and stored at −80°C. Virus was used at a titer of 10^7 particles/μl. Mice were given metamizol (3ml/L) in drinking water for 2 days prior to surgery and up to 3 days after. On the day of surgery, mice were anesthetized with a single intraperitoneal injection of ketamine/xylazine (80 and 10 mg/kg, respectively) and given a single subcutaneous injection of buprenorphine (0.1 mg/kg). Mice were fixed in a stereotaxic device (myNeuroLab Wetzlar, Germany), an incision was made to expose the bone and anteroposterior (−1.75mm) and mediolateral (±1.0 mm) coordinates from bregma were used for drilling holes bilaterally. A fine glass injection capillary filled with 1.2 μl virus was then slowly lowered to −1.5 (dorsoventral) and allowed to rest for 1 min. 0.9 μl was then injected over 3 min. The needle was allowed to rest in place for an additional minute after the injection and then slowly lifted above bone level. This procedure was repeated for both hippocampi. Mice were then removed from the stereotaxic device and tissue glue (Histoacryl, B Braun) was used to seal the wound. They were then allowed to recover on a heat blanket and transferred to individual cages for post-operation recovery. Mice were given buprenorphin injections up to 2 days after the operation and closely monitored for signs of distress or pain. Mice were only used for subsequent experiment after a minimum of 2 weeks post-operation.

Electrophysiological recordings from dissociated hippocampal neurons

Following transfection on DIV10, DIV13-20 rat neurons growing on coverslips were placed in a custom-made recording chamber in extracellular solution containing, in mM: 142 NaCl, 2.5 KCl, 10 HEPES, 10 D-Glucose, 2 $CaCl_2$, 1.3 $MgCl_2$ (295 mOsm, pH adjusted to 7.2 with NaOH). The temperature of the bath was maintained at 30 to 32°C. To record miniature excitatory postsynaptic currents (mEPSCs), 1 μM TTX (to block action potentials) and 50 μM picrotoxin (to inhibit $GABA_A$ receptors) was added to the extracellular solution. An Olympus upright BX51WI microscope equipped with a 40X water-immersion objective, fluorescent light source (Lumen 200Pro, Prior Scientific), and filters for GFP fluorescence imaging were used to visualize neurons transfected with GFP, GFP-Syt3 or Turbo GFP-expressing Syt3 knockdown constructs. Patch pipettes were pulled from borosilicate glass (1.5 mm OD, 0.86 mm ID, 3 to 6 megohms) using a P-97 micropipette puller (Sutter Instruments). The internal solution contained, in mM: 130 K-gluconate, 10 NaCl, 1 EGTA, 0.133 $CaCl_2$, 2 $MgCl_2$, 10 HEPES, 3.5 Na_2-ATP,1 Na-GTP (285 mOsm, pH adjusted to 7.4 with KOH). Whole-cell patch-clamp recordings were obtained using a HEKA EPC10 USB double patch clamp amplifier coupled to Patchmaster acquisition software. Signals were low pass filtered using a Bessel filter at 2.9 KHz and digitized at 5 KHz. mEPSCs were recorded while holding neurons at −60 mV in the voltage-clamp mode, with fast and slow capacitance, and series resistance compensated. The series resistance was monitored during recording to ensure it did not change by more than ± 3 megohms and neurons were recorded from only if uncompensated Rs < 20 megohms. MEPSCs were analyzed using Mini Analysis software v6.0.3 (Synaptosoft Inc.) with an amplitude threshold of 3.5 X average RMS noise.

DIV13-19 mouse neurons were recorded from in the same conditions except the bath was at room temperature, and 100 μM picrotoxin was added. For AMPA stimulation, coverslips were transferred to 250 μl prewarmed medium containing 100 μM S-AMPA (Abcam ab120005) and incubated at 37°C and 5% CO_2 for 2 min, followed by 8 min incubation in conditioned medium without AMPA, as for receptor internalization assays. Whole cell recordings were performed on an upright microscope (Zeiss Examiner D1) equipped with a 40X water immersion objective with a fluorescent light source (Zeiss Colibri) using an ELC-03XS patch clamp amplifier (NPI Electronics, Germany) with custom written data acquisition scripts for IgorPro 6.12A software (Wavemetrics), from Oliver Schlüter (European Neuroscience Institute, Goettingen). Signals were digitized at 10 KHz using an InstruTECH ITC-18 data acquisition interface (HEKA). The fast capacitance was compensated and slow capacitance and series resistance were not compensated. The series resistance did not change by more than 10%, monitored every 10 s. The experimenter was blinded to file names during analysis.

Whole-cell electrophysiology in acute hippocampal slices

Patch pipettes with a resistance of 2.5 to 5 megohms were prepared from glass capillaries (Harvard Apparatus, cat. no. 300060, 1.5 mm OD, 0.86 mm ID) using a P-97 puller (Sutter Inst, Novato, CA). P12-P17 male and female mouse pups were anesthetized with isoflurane (Abbott, Wiesbaden, Germany), decapitated, and the brain extracted and transferred to cold NMDG buffer containing (in mM) 45 NMDG, 0.33 KCl, 0.4 KH_2PO_4, 0.5 $MgCl_2$, 0.16 $CaCl_2$, 20 choline bicarbonate, 12.95 glucose. 300 μm coronal hippocampal slices were made with a Leica VT1200 vibratome (Wetzlar, Germany) and a stainless steel blade (Feather) in ice cold NMDG buffer. Slices were transferred to a preincubation chamber with a mesh bottom filled with ACSF containing (in mM) 124 NaCl, 4.4 KCl, 1 NaH_2PO_4, 26.2 $NaHCO_3$, 1.3 $MgSO_4$, 2.5 $CaCl_2$, and 10 D-Glucose, bubbled with 95% O_2/5% CO_2 (carbogen) and incubated at 35°C for 0.5 hours followed by another 0.5 hours at room temperature. Hippocampi were then dissected using a Zeiss Stemi 2000 stereoscopic microscope. A cut perpendicular to the CA3 pyramidal cell layer was made in the CA3 region and another cut perpendicular to the CA1 field at the medial end of the slice was made to prevent recurrent activity. Slices were submerged in a chamber perfused with carbogen-bubbled ACSF maintained at 30°C-32°C and CA1 neurons visualized with an upright Zeiss Examiner D1 microscope equipped with a 40X water-immersion objective. The intracellular pipette solution contained (in millimolar) 130 $CsMeSO_3$, 2.67 CsCl, 10 HEPES, 1 EGTA, 4 Mg-ATP, 0.3 Na-GTP, 3 QX-314 Cl, 5 TEA-Cl, 15 Phosphocreatine disodium, and 5 U/ml Creatine-phosphokinase (mOsm, 303; pH, 7.44). Whole-cell patch-clamp recordings were obtained using a NPI ELC-03XS patch clamp amplifier and digitized using an InstruTECH ITC-18 data acquisition interface (HEKA). A custom written procedure (provided by Oliver Schlüter, European Neuroscience Institute Goettingen) in Igor Pro 6.12A was used to visualize and store recorded data. Signals were low pass filtered using a Bessel filter at 3 KHz and digitized at 10 KHz. Schaffer collaterals were stimulated at 0.1 Hz using a bipolar glass electrode filled with ACSF at the distal dendritic region of the stratum radiatum close to the border of the lacunosum-moleculare, and a minimum of 30 EPSCs were averaged. The fast capacitance was compensated and slow capacitance and series resistance were not compensated. Synaptic responses were first recorded at a holding potential of −56 mV, the measured average reversal potential for Cl^- in wild-type slices. $GABA_A$ receptor-mediated currents were then recorded at 0 mV, the measured average reversal potential of NMDA and AMPA receptors. 0.1 mM picrotoxin was then perfused while holding at −56 mV after which the elimination of GABA IPSCs at 0 mV was confirmed. The residual AMPA+NMDA EPSC at 0 mV was then subtracted from the GABA IPSC. The AMPA EPSCs subsequently recorded at −56 mV, which were free of any $GABA_A$ receptor IPSC component, were used for analysis. The AMPA+NMDA compound EPSC was then recorded at +40 mV in the presence of 0.1 mM picrotoxin, where the amplitude of the EPSC approximately 60 ms after the peak of the AMPA

EPSC is considered to be purely NMDA receptor-mediated, since the measured AMPA receptor EPSC decay time constant $\tau \approx 20$ ms. The input and series resistance (Rs) were monitored every 10 s. Recordings where Rs was > 25 megohms or changed by more than ± 20% during recording were excluded from analysis. Input resistances ranged from 100 to 400 megohms and did not change by more than ± 20% during the course of the recording. Matlab was used to calculate current ratios and decay times.

Extracellular recordings from acute hippocampal slices

Acute hippocampal slices were prepared from 8 to 12-week-old male mice anesthetized with isoflurane and decapitated. The hippocampus was removed and 400 μm thick dorsal hippocampal slices were cut transversely using a tissue chopper (Stoelting) in ice-cold artificial cerebrospinal fluid (ACSF) containing, in mM: 124 NaCl, 4.9 KCl, 1.2 KH_2PO_4, 2 $MgSO_4$, 2 $CaCl_2$, 24.6 $NaHCO_3$, and 10 D-glucose (saturated with 95% O_2 and 5% CO_2, pH 7.4, ~305 mOsm). Within 5 min of decapitation, slices were transferred to a custom-built interface chamber and pre-incubated in ACSF for at least 3 hours. Following pre-incubation, the stimulation strength was set to elicit 40% of the maximal field EPSP (fEPSP) slope. The slope of the rising phase of the fEPSP was used to determine potentiation of synaptic responses. For stimulation, biphasic constant current pulses were used. A baseline was recorded for at least 30 min before LTD or LTP induction. Four averaged 0.2 Hz biphasic, constant-current pulses (0.1 ms per polarity) were used to test responses post-tetanus for up to 4 hours.

LTD was induced by a single tetanus of 900 pulses at 1 Hz. Nondecaying LTP was induced by a 3XTET high frequency stimulation with three stimulus trains of 100 pulses at 100 Hz, stimulus duration 0.2 ms per polarity with 10 min intertrain intervals (*50*). Decaying LTP was induced with a 1XTET single tetanus of 16 pulses at 100 Hz, stimulus duration 0.2 ms per polarity, modified for mouse hippocampal slices from the protocol consisting of 21 pulses used for rat hippocampal slices (*36*). The Tat-GluA2-3Y peptide (sequence YGRKKRRQRRR-$_{869}$YKEGYNVYG$_{877}$, provided by Yu-Tian Wang, University of British Columbia, Vancouver, Canada) was used at a concentration of 1 μM and ZIP (Tocris cat. no. 2549) was dissolved in water, as recommended by the manufacturer, and used at a concentration of 1 μM (*13*). Control and experimental recordings were interleaved as much as possible for comparison of conditions. For each condition, the corresponding control was repeated before and intermittently throughout experiments, to ensure consistent recording conditions.

Behavioral experiments

Behavioral experiments were performed on 3- to 9-month-old male mice by a male experimenter, except for the Barnes maze, where a male experimenter performed intraperitoneal injections and a female experimenter performed experiments. All experimenters were blinded to genotype. Mice were individually housed at the European Neuroscience Institute Göttingen, Germany animal facility in standard environmental conditions (temperature, humidity), with ad libitum access to food and water and a 12 hours light/dark cycle. Mice were allowed to habituate to different holding rooms for behavioral experiments for two weeks before testing, and to experimenters for at least three days before experiments . All experiments were performed during the light cycle. Video tracking was done with the TSE monitoring system Videomot2. All behavioral experiments were approved under project number G15.1794 by the Niedersächsisches Landesamt für Verbraucherschutz und Lebensmittelsicherheit (LAVES, Lower Saxony, Germany).

Open field, elevated plus maze

In the open field test, mice were introduced near the wall of an empty, opaque square plexiglas box and allowed to freely explore the arena for 5 min. Before every trial, urine was removed with Kimwipes, and the arena was cleaned with water and 70% EtOH. Time spent in the center (2 × 2 grid in the middle of a 4 × 4 grid arena) relative to near the walls, and the total path travelled was recorded.

For the elevated plus maze, mice were introduced into the center quadrant of a 4-arm maze with two open and two closed arms Before every trial, urine was removed with Kimwipes, and the maze was cleaned with water and 70% EtOH. Time spent in the open arms was analyzed.

Reference memory water maze

Näive mice from four independent cohorts were trained to find a 13 × 13 cm square hidden platform (uninjected mice) or a 10 cm diameter circular platform (injected mice) submerged 1.5 cm below the surface in a 1.1 m diameter circular pool filled with white opaque water at 19 ± 1°C. Mice were trained in 4 trials per day in succession where each trial lasted 1 min during which the mice searched for the platform. A trial ended when the mouse spent at least 2 s on the platform, after which they were left on the platform for 15 s prior to the start of the next trial. Four shapes around the pool (star, square, triangle, circle) served as visual cues. Mice that failed to find the platform after 1 min were guided to it and left on the platform for 15 s. Mice that failed to swim (floaters) were excluded from analysis. Mice were placed into the pool facing the wall at the beginning of each trial, and the position of pool entry from four different directions was randomly shuffled daily. For probe tests, the platform was removed and mice were placed into the pool near the wall in the quadrant opposite to that of the platform location and allowed to search for the platform for 1 min. Two probe tests were performed to monitor learning of the first platform position and additional probe test(s) performed after reversal, i.e., switching the platform position to the opposite quadrant. Only data from coincident days of training from the first 2 cohorts (Fig. 5, A to F) was pooled. Video tracking data was analyzed using Matlab to extract time-tagged xy-coordinate information and quantify escape latency, platform crossings, proximity [mean distance of all tracked path points to platform center, which is reported to be the most reliable parameter to quantify spatial specificity of water maze search patterns (*41*)], percent time spent in target quadrant, and average swimming speed. Occupancy plots were generated by super-imposing all path points of all mice in a group. Densities of path points (normalized to total number of path points in a group of mice) within a grid size of 2.1 cm × 2.1 cm (*43*) were calculated. Density data was smoothened and interpolated to plot heat maps (Scattercloud function, Matlab File ID 6037). Occupancy plot color maps were linearly scaled using the global minimum and maximum densities for all groups, to allow comparison between them. The last 0.5 s of the trial, when mice were on the platform and not searching, was excluded in occupancy plots for Fig. 5G. To generate occupancy plots of probe trials from two cohorts, in which the platform was in different positions (Fig. 5, E and F), the tracking data from one cohort was transposed and mirror imaged with respect to the center pool line and superimposed on data from the second cohort. Circular areas encompassing platforms of both cohorts in both original and reversal quadrants were defined as target areas.

Because forgetting cannot be analyzed in mice that did not learn, mice in i.p. injected cohorts (which learned more slowly) were excluded from analysis if (i) their swim speed was less than 6.2 cm/s for more than three consecutive days, (ii) their proximity or escape latency failed to decrease between the first day of training and the average of the last three days of training before platform reversal, or (iii) they spent 0% time in the target quadrant in the second probe test. These criteria were also met by all other cohorts tested. Daily i.p. injections (maximum volume injected, 10 μl/g body weight) were performed 1 hour before training (*13*). Mice were injected with saline (0.9% NaCl) during training to the first platform position and then injected with saline or with Tat-GluA2-3Y peptide (5 μmol/kg body weight) one hour before the second probe test and daily after reversal. Probe tests following reversal training of i.p. injected cohorts were performed on three consecutive days.

Delayed matching to place water maze

The delayed matching-to-place task protocol was performed as previously described (*42*) with modifications. Mice were first habituated to the task by training to a visible platform (marked by a graduated cylinder coated with multi-colored paper on top of a submerged platform) placed at a unique position every day for 3 days in a 1.1 m diameter circular pool filled with white opaque water at 19 ± 1°C. The circular platform was submerged 1.5 cm below the surface and had a radius of 5 cm. Four shapes around the pool (star, square, triangle, circle) served as visual cues. After habituation, mice were trained to 16 unique hidden platform positions at two fixed distances

from the pool center (11 in an outer ring and 5 in an inner ring) over 16 days. Mice underwent 4 trials of 2 min every day. The platform was shifted to a new random position every day in a different quadrant alternating between inner and outer rings as much as possible. A trial ended when the mouse spent at least 2 s on the platform, after which they were left on the platform for 15 s and then returned to their home cage. Mice were warmed with infrared lamps after every trial. The drop-off points with respect to the platform position of that day were in a random order. Mice were divided into two groups for counterbalancing in which each group experienced different alternations of platform positions between inner and outer rings, to prevent non-spatial chaining search strategies in which mice search for platforms within a certain distance of the pool wall. Inter-trial intervals were 5 min; from day 10 onwards, the inter-trial interval between trial 1 and trial 2 was increased to 1 hour 15 min. Trial 2 on day 16 was a probe trial, i.e., the platform was removed and the exploratory behavior of mice recorded for 2 min. Because the platform in this trial was missing, only the search path data before the first crossing of the platform position from trial 1 was used to calculate savings of proximity, escape latency and path length. All mice were trained at the same time of the day as far as possible, i.e., some mice were always trained in the morning while others were always trained in the evening. In all occupancy plots, the last 1.5 s of the trial were excluded to enhance contrast in the pool and avoid high occupancy densities on the platform, since all mice spent the last 2 s of every trial on the platform.

Quantitation of search strategy was modified from a previously described method (*43*). A Matlab script extracted time-tagged xy-coordinate information from video tracking data of all trials and classified individual trials as search strategies. The following parameters were used for classification of the indicated search strategies. Direct swimming strategy: total path length ≤1.4 X distance between drop-off point and platform center, ≥80% path points within a 30° goal corridor angle; Focal search strategy: mean proximity to platform center ≤0.35 X pool radius, mean proximity to path centroid ≤0.4 X pool radius; Directed search strategy: ≥70% path points within a 30° goal corridor angle; Perseverance strategy: mean proximity to previous platform center ≤0.5 X pool radius, mean proximity to path centroid allowed for perseverance ≤0.6 X pool radius; Chaining strategy: ≥70% path points inside annulus around the ring of platforms (inner or outer) containing the current day's platform, by 0.01 to 0.02 X pool radius, annulus for platforms in outer ring between 0.52 X pool radius and 0.73 X pool radius, annulus for platforms in inner ring between 0.22 X pool radius and 0.42 X pool radius; Scanning strategy: ≥80% of path points inside scanning radius (a circular area enclosing all platforms, 0.73 X pool radius), total % pool area scanned ≥10% and ≤50%; Thigmotaxis: ≥30% of path points inside closer wall zone starting 0.85 X pool radius and ≥50% of path points inside wider wall zone starting 0.75 X pool radius; Random Search strategy: % pool area scanned ≥50%.

Barnes Maze

The Barnes maze consisted of a white circular platform made of plexiglass, 92cm in diameter, with 20 equally spaced holes (5 cm in diameter) along the perimeter. The platform was elevated 40 cm above the ground. An escape chamber ($15.5 \times 9 \times 6$ cm^3) was placed under one of the holes, defined as the target hole. To encourage mice to enter the escape chamber, it contained a plastic ramp to enable the mice to climb into it and an odorless paper towel, resembling nesting material. Before every trial, urine was removed with Kimwipes, and the arena was cleaned with water and 70% EtOH to eliminate olfactory cues. For each trial a mouse was placed onto the middle of the maze, such that the target hole was not distinguishable from any other hole and the mouse had to rely on three visual cues (26×26 cm^2 in size) placed 5 cm from the edge of the platform to identify the location of the target hole. The platform was uniformly illuminated by bright LED light which served as a mildly aversive stimulus to motivate the mice to search for the target hole.

Daily i.p. injections (maximum volume injected, 10 µl/g body weight) were performed one hour before training (*13*). Mice were injected with saline (0.9% NaCl) during training to the first hole position and then injected with saline or with Tat-GluA2-3Y peptide (5 µmol/kg body weight) one hour before the second probe test and daily after reversal.

On the day before training, mice were habituated to the maze by placing them in a clear plastic cylinder (15 cm in diameter) in the middle of the platform for 30 s, before gently guiding them to the target hole, where they were given 3 min to enter the escape chamber. If mice did not enter the escape chamber, they were gently nudged with the cylinder into the chamber. All mice spent 1 min in the escape chamber before being returned to their home cage. On subsequent training days, mice were placed into an opaque plastic cylinder (15 cm in diameter) covered by an opaque lid for 15 s to randomize starting orientation. Each trial, lasting 2 min, was initiated after lifting the cylinder. If the mouse climbed into the escape chamber, the trial was stopped and the mouse returned to its home cage after remaining inside the escape chamber for 1 min. If the mouse did not climb into the escape chamber within 2 min, it was gently guided to the target hole with the clear plastic cylinder and given 3 min to climb into the escape chamber, where it remained for 1 min, before being returned to its home cage.

In probe tests, the escape chamber was removed, and mice were allowed to explore the maze for 2 min. The "reversal" hole was located in an adjacent quadrant, since some mice showed a bias toward exploring the opposite quadrant during initial training. Mice experienced one trial per day, and were given a one-day "break" after the first three probe tests, during which they did not perform in the Barnes maze, but still received saline (maximum volume injected, 10 µl 0.9% NaCl/g body weight) or GluA2-3Y (5 µmol/kg body weight) i.p. injections.

Three-point (head, center, tail) tracking data was exported into Matlab for further analysis. Occupancy plots were generated using Matlab as described above for the water maze, except that head instead of center coordinates were used. Video tracking errors in which head and tail coordinates were erroneously swapped (mostly close to hole regions) were detected by a distance threshold and excluded. Mice that did not find the original target hole in either of the first two probe tests (did not learn the target hole) were excluded from analysis of perseverance after reversal. Target area was defined as the area of the target hole and its two neighboring holes using center tracked coordinates, for calculation of the perseverance ratio (time spent in reversal target area divided by total time spent in original and reversal target areas).

Statistical analysis

All statistical analysis was done using GraphPad Prism or Microsoft Excel. All reported values in statistical analysis represent the mean, error bars indicate SEM, and all Student's t tests are two-tailed type 2, unless otherwise indicated. For all statistical tests, data met the assumptions of the test. All n numbers listed in Figure Legends refer to biological replicates.

REFERENCES AND NOTES

1. J. M. Henley, K. A. Wilkinson, Synaptic AMPA receptor composition in development, plasticity and disease. *Nat. Rev. Neurosci.* **17**, 337–350 (2016). doi: 10.1038/nrn.2016.37; pmid: 27080385
2. J. D. Shepherd, R. L. Huganir, The cell biology of synaptic plasticity: AMPA receptor trafficking. *Annu. Rev. Cell Dev. Biol.* **23**, 613–643 (2007). doi: 10.1146/annurev.cellbio.23.090506.123516; pmid: 17506699
3. G. L. Collingridge, J. T. Isaac, Y. T. Wang, Receptor trafficking and synaptic plasticity. *Nat. Rev. Neurosci.* **5**, 952–962 (2004). doi: 10.1038/nrn1556; pmid: 15550950
4. R. C. Malenka, M. F. Bear, LTP and LTD: An embarrassment of riches. *Neuron* **44**, 5–21 (2004). doi: 10.1016/j.neuron.2004.09.012; pmid: 15450156
5. S. Nabavi *et al*., Engineering a memory with LTD and LTP. *Nature* **511**, 348–352 (2014). doi: 10.1038/nature13294; pmid: 24896183
6. T. J. Ryan, D. S. Roy, M. Pignatelli, A. Arons, S. Tonegawa, Memory. Engram cells retain memory under retrograde amnesia. *Science* **348**, 1007–1013 (2015). doi: 10.1126/science.aaa5542; pmid: 26023136
7. J. H. Choi *et al*., Interregional synaptic maps among engram cells underlie memory formation. *Science* **360**, 430–435 (2018). doi: 10.1126/science.aas9204; pmid: 29700265
8. P. V. Migues *et al*., Blocking synaptic removal of GluA2-containing AMPA receptors prevents the natural forgetting of long-term memories. *J. Neurosci.* **36**, 3481–3494 (2016). doi: 10.1523/JNEUROSCI.3333-15.2016; pmid: 27013677
9. A. Hayashi-Takagi *et al*., Labelling and optical erasure of synaptic memory traces in the motor cortex. *Nature* **525**, 333–338 (2015). doi: 10.1038/nature15257; pmid: 26352471
10. R. Scholz *et al*., AMPA receptor signaling through BRAG2 and Arf6 critical for long-term synaptic depression. *Neuron* **66**, 768–780 (2010). doi: 10.1016/j.neuron.2010.05.003; pmid: 20547133
11. G. Ahmadian *et al*., Tyrosine phosphorylation of GluR2 is required for insulin-stimulated AMPA receptor endocytosis and LTD. *EMBO J.* **23**, 1040–1050 (2004). doi: 10.1038/sj.emboj.7600126; pmid: 14976558

12. P. V. Migues *et al*., PKMzeta maintains memories by regulating GluR2-dependent AMPA receptor trafficking. *Nat. Neurosci.* **13**, 630–634 (2010). doi: 10.1038/nn.2531; pmid: 20383136
13. Z. Dong *et al*., Long-term potentiation decay and memory loss are mediated by AMPAR endocytosis. *J. Clin. Invest.* **125**, 234–247 (2015). doi: 10.1172/JCI77888; pmid: 25437879
14. M. Y. Xiao, Y. P. Niu, H. Wigström, Activity-dependent decay of early LTP revealed by dual EPSP recording in hippocampal slices from young rats. *Eur. J. Neurosci.* **8**, 1916–1923 (1996). doi: 10.1111/j.1460-9568.1996.tb01335.x; pmid: 8921282
15. D. M. Villarreal, V. Do, E. Haddad, B. E. Derrick, NMDA receptor antagonists sustain LTP and spatial memory: Active processes mediate LTP decay. *Nat. Neurosci.* **5**, 48–52 (2002). doi: 10.1038/nn776; pmid: 11740500
16. M. D. Ehlers, Reinsertion or degradation of AMPA receptors determined by activity-dependent endocytic sorting. *Neuron* **28**, 511–525 (2000). doi: 10.1016/S0896-6273(00)00129-X; pmid: 11144360
17. E. C. Beattie *et al*., Regulation of AMPA receptor endocytosis by a signaling mechanism shared with LTD. *Nat. Neurosci.* **3**, 1291–1300 (2000). doi: 10.1038/81823; pmid: 11100150
18. D. Wu *et al*., Postsynaptic synaptotagmins mediate AMPA receptor exocytosis during LTP. *Nature* **544**, 316–321 (2017). doi: 10.1038/nature21720; pmid: 28355182
19. R. B. Sutton, B. A. Davletov, A. M. Berghuis, T. C. Südhof, S. R. Sprang, Structure of the first C2 domain of synaptotagmin I: A novel Ca^{2+}/phospholipid-binding fold. *Cell* **80**, 929–938 (1995). doi: 10.1016/0092-8674(95)90296-1; pmid: 7697723
20. S. Butz, R. Fernandez-Chacon, F. Schmitz, R. Jahn, T. C. Südhof, The subcellular localizations of atypical synaptotagmins III and VI. Synaptotagmin III is enriched in synapses and synaptic plasma membranes but not in synaptic vesicles. *J. Biol. Chem.* **274**, 18290–18296 (1999). doi: 10.1074/jbc.274.26.18290; pmid: 10373432
21. T. C. Südhof, Synaptotagmins: Why so many? *J. Biol. Chem.* **277**, 7629–7632 (2002). doi: 10.1074/jbc.R100052200; pmid: 11739399
22. S. Sugita, O. H. Shin, W. Han, Y. Lao, T. C. Südhof, Synaptotagmins form a hierarchy of exocytotic Ca(2+) sensors with distinct Ca(2+) affinities. *EMBO J.* **21**, 270–280 (2002). doi: 10.1093/emboj/21.3.270; pmid: 11823420
23. C. Dean *et al*., Axonal and dendritic synaptotagmin isoforms revealed by a pHluorin-syt functional screen. *Mol. Biol. Cell* **23**, 1715–1727 (2012). doi: 10.1091/mbc.e11-08-0707; pmid: 22398727
24. L. W. Gong, P. De Camilli, Regulation of postsynaptic AMPA responses by synaptojanin 1. *Proc. Natl. Acad. Sci. U.S.A.* **105**, 17561–17566 (2008). doi: 10.1073/pnas.0809221105; pmid: 18987319
25. D. T. Lin, R. L. Huganir, PICK1 and phosphorylation of the glutamate receptor 2 (GluR2) AMPA receptor subunit regulates GluR2 recycling after NMDA receptor-induced internalization. *J. Neurosci.* **27**, 13903–13908 (2007). doi: 10.1523/JNEUROSCI.1750-07.2007; pmid: 18077702
26. J. Boyken *et al*., Molecular profiling of synaptic vesicle docking sites reveals novel proteins but few differences between glutamatergic and GABAergic synapses. *Neuron* **78**, 285–297 (2013). doi: 10.1016/j.neuron.2013.02.027; pmid: 23622064
27. M. Rathje *et al*., AMPA receptor pHluorin-GluA2 reports NMDA receptor-induced intracellular acidification in hippocampal neurons. *Proc. Natl. Acad. Sci. U.S.A.* **110**, 14426–14431 (2013). doi: 10.1073/pnas.1312982110; pmid: 23940334
28. T. A. Blanpied, D. B. Scott, M. D. Ehlers, Dynamics and regulation of clathrin coats at specialized endocytic zones of dendrites and spines. *Neuron* **36**, 435–449 (2002). doi: 10.1016/S0896-6273(02)00979-0; pmid: 12408846
29. J. Lu *et al*., Postsynaptic positioning of endocytic zones and AMPA receptor cycling by physical coupling of dynamin-3 to Homer. *Neuron* **55**, 874–889 (2007). doi: 10.1016/j.neuron.2007.06.041; pmid: 17880892
30. E. M. Petrini *et al*., Endocytic trafficking and recycling maintain a pool of mobile surface AMPA receptors required for synaptic potentiation. *Neuron* **63**, 92–105 (2009). doi: 10.1016/j.neuron.2009.05.025; pmid: 19607795
31. M. Rosendale, D. Jullié, D. Choquet, D. Perrais, Spatial and temporal regulation of receptor endocytosis in neuronal dendrites revealed by imaging of single vesicle formation. *Cell Reports* **18**, 1840–1847 (2017). doi: 10.1016/j.celrep.2017.01.081; pmid: 28228251
32. S. H. Lee, L. Liu, Y. T. Wang, M. Sheng, Clathrin adaptor AP2 and NSF interact with overlapping sites of GluR2 and play distinct roles in AMPA receptor trafficking and hippocampal LTD. *Neuron* **36**, 661–674 (2002). doi: 10.1016/S0896-6273(02)01024-3; pmid: 12441055
33. W. Lu *et al*., Subunit composition of synaptic AMPA receptors revealed by a single-cell genetic approach. *Neuron* **62**, 254–268 (2009). doi: 10.1016/j.neuron.2009.02.027; pmid: 19409270
34. J. W. Lin *et al*., Distinct molecular mechanisms and divergent endocytotic pathways of AMPA receptor internalization. *Nat. Neurosci.* **3**, 1282–1290 (2000). doi: 10.1038/81814; pmid: 11100149
35. Z. Dong *et al*., Hippocampal long-term depression mediates spatial reversal learning in the Morris water maze. *Neuropharmacology* **64**, 65–73 (2013). doi: 10.1016/j.neuropharm.2012.06.027; pmid: 22732443
36. S. Sajikumar, S. Navakkode, J. U. Frey, Identification of compartment- and process-specific molecules required for "synaptic tagging" during long-term potentiation and long-term depression in hippocampal CA1. *J. Neurosci.* **27**, 5068–5080 (2007). doi: 10.1523/JNEUROSCI.4940-06.2007; pmid: 17494693
37. P. Tsokas *et al*., Compensation for PKMζ in long-term potentiation and spatial long-term memory in mutant mice. *eLife* **5**, e14846 (2016). doi: 10.7554/eLife.14846; pmid: 27187150
38. Y. Yao *et al*., PKM zeta maintains late long-term potentiation by N-ethylmaleimide-sensitive factor/GluR2-dependent trafficking of postsynaptic AMPA receptors. *J. Neurosci.* **28**, 7820–7827 (2008). doi: 10.1523/JNEUROSCI.0223-08.2008; pmid: 18667614
39. N. Sadeh, S. Verbitsky, Y. Dudai, M. Segal, Zeta Inhibitory Peptide, a candidate inhibitor of protein kinase Mζ, is excitotoxic to cultured hippocampal neurons. *J. Neurosci.* **35**, 12404–12411 (2015). doi: 10.1523/JNEUROSCI.0976-15.2015; pmid: 26354909
40. M. J. LeBlancq, T. L. McKinney, C. T. Dickson, ZIP It: Neural silencing is an additional effect of the PKM-ζ inhibitor zeta-inhibitory peptide. *J. Neurosci.* **36**, 6193–6198 (2016). doi: 10.1523/JNEUROSCI.4563-14.2016; pmid: 27277798
41. H. R. Maei, K. Zaslavsky, C. M. Teixeira, P. W. Frankland, What is the most sensitive measure of water maze probe test performance? *Front. Integr. Nuerosci.* **3**, 4 (2009). doi: 10.3389/neuro.07.004.2009; pmid: 19404412
42. K. Nakazawa *et al*., Hippocampal CA3 NMDA receptors are crucial for memory acquisition of one-time experience. *Neuron* **38**, 305–315 (2003). doi: 10.1016/S0896-6273(03)00165-X; pmid: 12718863
43. A. Garthe, J. Behr, G. Kempermann, Adult-generated hippocampal neurons allow the flexible use of spatially precise learning strategies. *PLOS ONE* **4**, e5464 (2009). doi: 10.1371/journal.pone.0005464; pmid: 19421325
44. A. Citri *et al*., Calcium binding to PICK1 is essential for the intracellular retention of AMPA receptors underlying long-term depression. *J. Neurosci.* **30**, 16437–16452 (2010). doi: 10.1523/JNEUROSCI.4478-10.2010; pmid: 21147983
45. M. Fiuza *et al*., PICK1 regulates AMPA receptor endocytosis via direct interactions with AP2 α-appendage and dynamin. *J. Cell Biol.* **216**, 3323–3338 (2017). doi: 10.1083/jcb.201701034; pmid: 28855251
46. J. Yao, S. E. Kwon, J. D. Gaffaney, F. M. Dunning, E. R. Chapman, Uncoupling the roles of synaptotagmin I during endo- and exocytosis of synaptic vesicles. *Nat. Neurosci.* **15**, 243–249 (2011). doi: 10.1038/nn.3013; pmid: 22197832
47. G. A. Banker, W. M. Cowan, Rat hippocampal neurons in dispersed cell culture. *Brain Res.* **126**, 397–42 (1977). doi: 10.1016/0006-8993(77)90594-7; pmid: 861729
48. J. Rizo, T. C. Südhof, C2-domains, structure and function of a universal Ca2+-binding domain. *J. Biol. Chem.* **273**, 15879–15882 (1998). doi: 10.1074/jbc.273.26.15879; pmid: 9632630
49. A. Bhalla, M. C. Chicka, E. R. Chapman, Analysis of the synaptotagmin family during reconstituted membrane fusion. Uncovering a class of inhibitory isoforms. *J. Biol. Chem.* **283**, 21799–21807 (2008). doi: 10.1074/jbc.M709628200; pmid: 18508778
50. U. Frey, R. G. Morris, Weak before strong: Dissociating synaptic tagging and plasticity-factor accounts of late-LTP. *Neuropharmacology* **37**, 545–552 (1998). doi: 10.1016/S0028-3908(98)00040-9; pmid: 9704995

ACKNOWLEDGMENTS

We thank R. Morris for recommendations of intertrial intervals in the DMP task, H. Urbanke for the Barnes maze protocol, and J. Schrader for technical assistance. **Funding:** This work was supported by a Sofja Kovalevskaja grant from the Alexander von Humboldt Foundation, European Research Council (ERC) starting grant SytActivity FP7 260916, and Deutsche Forschungsgemeinschaft (DFG) grants DE1951/1 and -3 and the Center for Nanoscale Microscopy and Molecular Physiology of the Brain (CNMPB) to C.D.; DFG research group KFO241/PsyCourse Fi981-4/Fi981 11-1, DFG project 179/1-1/2013, ERC consolidator grant DEPICODE 648898, BMBF projects ENERGI (01GQ1421A), and Intergrament 01ZX1314D, and funds from the German Center for Neurodegenerative Diseases to A.F.; Canadian Institute for Health Research grant FDN-154286 to Y.T.W.; and a Dorothea Schloezer fellowship to K.B. **Author contributions:** A.A. coordinated the project; designed, conducted, and analyzed all behavior experiments; designed and conducted receptor and Syt3 internalization assays and immunocytochemistry experiments of Syt3/endocytic zones and PSDs; conducted and analyzed pHluorin-Syt3 experiments; conducted and trained and supervised A.H. in mEPSC recordings; trained and supervised N.N. in whole-cell recordings from hippocampal slices and S.R. in Barnes maze behavior experiments; and revised the manuscript. B.R. designed, conducted, and analyzed all LTP, LTD, and field recording experiments and conducted all immunohistochemistry experiments. S.A. designed, conducted, and analyzed all biochemistry experiments. E.B. designed behavior experiments, trained A.A. in behavior experiments, and performed all hippocampal viral injections. Y.S. designed, conducted, and analyzed immunocytochemistry experiments of Syt3 localization and all pHluorin-Syt3 experiments. N.N. conducted and analyzed whole-cell recordings from hippocampal slices. A.H. conducted and analyzed mEPSC recordings. S.R. conducted and analyzed Barnes maze behavior experiments. H.M. designed, developed, and validated the Syt3 antibody. J.B. trained A.A. in and helped plan behavior experiments. K.B. performed biochemistry experiments. Y.T.W. generated and validated the GluA2-3Y peptide and helped plan behavior experiments. A.F. provided funding for J.B., and E.B. and helped plan behavior experiments. C.D. conceived and coordinated the project; provided funding for A.A., B.R., S.A., Y.S., and K.B.; conducted and analyzed receptor and Syt3 internalization assays and immunocytochemistry of Syt3, endocytic zones, and PSDs; and wrote and revised the manuscript. **Competing interests:** The authors declare no competing interests. **Data and materials availability:** All data are available in the manuscript or the supplementary materials.

SUPPLEMENTARY MATERIALS

www.sciencemag.org/content/363/6422/eaav1483/suppl/DC1
Figs. S1 to S8

18 August 2018; accepted 1 November 2018
Published online 13 December 2018
10.1126/science.aav1483

Science

Synaptotagmin-3 drives AMPA receptor endocytosis, depression of synapse strength, and forgetting

Ankit Awasthi, Binu Ramachandran, Saheeb Ahmed, Eva Benito, Yo Shinoda, Noam Nitzan, Alina Heukamp, Sabine Rannio, Henrik Martens, Jonas Barth, Katja Burk, Yu Tian Wang, Andre Fischer and Camin Dean

Science **363** (6422), eaav1483.
DOI: 10.1126/science.aav1483originally published online December 13, 2018

Forgetting and receptor removal

The trafficking of AMPA receptors to and from the surface of postsynaptic membranes regulates synaptic strength and underlies learning and memory. Awasthi *et al.* found that the integral membrane protein synaptotagmin-3 (Syt3) is predominantly found on postsynaptic endocytic zones of neurons, where it promotes AMPA receptor internalization (see the Perspective by Mandelberg and Tsien). In Syt3 overexpressing or knockdown neurons, synaptic transmission and short-term plasticity were unchanged. However, in neurons from Syt3 knockout mice, synaptic long-term depression was abolished and decaying long-term potentiation endured. In Syt3 knockout mice, spatial learning was unaltered; however, these animals showed signs of impaired forgetting and relearning during the water maze spatial memory task.

Science, this issue p. eaav1483; see also p. 31